Atmos. Chem. Phys. Discuss., https://doi.org/10.5194/acp-2017-576
Manuscript under review for journal Atmos. Chem. Phys.
Discussion started: 5 July 2017

Atmospheric Chemistry and Physics Discussions

Bulk and Molecular-Level Characterization of Laboratory-Aged Biomass Burning Organic Aerosol from Oak Leaf and Heartwood Fuels

Claire F. Fortenberry[1], Michael J. Walker[1], Yaping Zhang[1], Dhruv Mitroo[1,a], William H. Brune[2], Brent J. Williams[1]

[1] Department of Energy, Environmental, and Chemical Engineering, Washington University in Saint Louis, Saint Louis, MO 63130, USA

[2] Department of Meteorology and Atmospheric Science, Pennsylvania State University, State College, PA 16801, USA

[a] Now at the Department of Atmospheric Sciences, Rosenstiel School of Marine and Atmospheric Sciences, University of Miami, Miami, FL 33149, USA

Correspondence to: Brent J. Williams (brentw@wustl.edu)

Abstract.

The chemical complexity of biomass burning organic aerosol (BBOA) greatly increases with photochemical aging in the atmosphere, necessitating controlled laboratory studies to inform field observations. In these experiments, BBOA from American white oak (*Quercus alba*) leaf and heartwood samples was generated in a custom-built emissions and combustion chamber and photochemically aged in a Potential Aerosol Mass (PAM) flow reactor. A Thermal desorption Aerosol Gas chromatograph (TAG) was used in parallel with a high-resolution time-of-flight Aerosol Mass Spectrometer (AMS) to analyze BBOA chemical composition at different levels of photochemical aging. Individual compounds were identified and integrated to obtain relative decay rates for key molecular components. A recently-developed chromatogram binning positive matrix factorization (PMF) technique was used to obtain mass spectral profiles for factors in TAG BBOA chromatograms, improving analysis efficiency and providing a more complete determination of unresolved complex mixture (UCM) components. Additionally, the recently characterized TAG decomposition window was used to track molecular fragments created by the thermal decomposition of thermally labile BBOA during sample desorption. We demonstrate that while most components of primary BBOA decrease with photochemical aging, certain components eluting within the TAG thermal decomposition window instead increase. Specifically, the increasing trend in decomposition *m/z* 44 (CO_2^+) signals formation of secondary organic aerosol (SOA) in the PAM reactor. Sources of *m/z* 60 ($C_2H_4O_2^+$), typically attributed to freshly-emitted BBOA in AMS field measurements, were also investigated. From the TAG chemical speciation and decomposition window data, we observed a decrease in *m/z* 60 with photochemical aging due to the decay of anhydrosugars (including levoglucosan) and other compounds, as well as an increase in *m/z* 60 due to the formation of thermally labile organic acids within the PAM reactor, which decompose during TAG sample desorption. When aging both types of BBOA (leaf and wood),

the AMS data exhibit a combination of these two contributing effects, causing limited change to the overall *m/z* 60 signal. Our observations demonstrate the importance of chemically-speciated data in fully understanding bulk aerosol measurements provided by the AMS in both laboratory and field studies.

1 Introduction

Atmospheric particulate matter (PM) negatively affects human health (e.g. Kampa and Castanas, 2008), impedes visibility (e.g. Appel et al., 1985), and can impact the global energy balance through direct radiative forcing or by acting as cloud condensation nuclei (e.g. Kanakidou et al., 2005). Organic aerosol (OA) composes 20-90% of submicron PM (PM_1) and is composed of thousands of distinct organic compounds (Goldstein and Galbally, 2007; Ng et al., 2010; Zhang et al., 2007). Given the multitude of organic compounds in the atmosphere and the numerous chemical reactions they can experience during atmospheric processing (e.g. Goldstein and Galbally, 2007; Kroll et al., 2009), laboratory studies are needed to obtain a complete understanding of the chemical composition and oxidative evolution of source-specific primary OA (POA, aerosol emitted directly into the atmosphere) and secondary OA (SOA, formed from gas-phase material that partition into the particle phase following photooxidation) components.

Biomass burning organic aerosol (BBOA) may contribute up to 90% of global combustion OA and 75% of combustion POA (Bond et al., 2004; May et al., 2013). Previous molecular-level BBOA studies over the past several decades have focused on the chemical composition of primary emissions (e.g. Fine et al., 2002; Oros and Simoneit, 1999; Rogge et al., 1998; Simoneit et al., 2000). In recent years, improved understanding of SOA formation in BBOA plumes has motivated the use of oxidation chambers in laboratory BBOA experiments (e.g. Cubison et al., 2011; Grieshop et al., 2009; Ortega et al., 2013). Some of these BBOA photooxidation studies have demonstrated that OA production can exceed decay under certain conditions due to oxidation and phase partitioning of gas-phase semivolatile and intermediately volatile compounds (SVOCs and IVOCs, respectively) (Grieshop et al., 2009). Other field measurements indicate minimal OA enhancement with aging of primary biomass plumes (Capes et al., 2008). During the third Fire Lab at Missoula Experiment (FLAME-3) campaign (2013), OA enhancements following photooxidation were shown to vary widely depending on the biomass source; while BBOA from some sources doubled in mass after photochemical aging, other types of BBOA were depleted (Ortega et al., 2013). The variation in OA enhancement observed by Ortega, et al. in the FLAME-3 study suggests that the amount of SOA from biomass emissions depends on the fuel type, illustrating the need for source-specific oxidation studies to investigate reactions and products leading to SOA formation.

Many previous BBOA oxidation studies (e.g. Grieshop et al., 2009; Ortega et al., 2013) have utilized a High-Resolution Time-Of-Flight Aerosol Mass Spectrometer (HR-ToF-AMS, Aerodyne, Inc., Billerica, MA). The Aerosol Mass Spectrometer (AMS) was developed to obtain chemical information on bulk aerosol including total mass concentrations and high-resolution ion signals, allowing for determination of bulk aerosol chemical composition (Canagaratna et al., 2007; DeCarlo et al., 2006). Hydrogen-to-carbon ratios (H:C) and oxygen-to-carbon ratios (O:C) can also be calculated using high-resolution AMS data, which are incorporated into estimations of an average carbon oxidation state ($\overline{OS_C} \approx 2{\times}H{:}C - O{:}C$; Kroll et al., 2011). Although the AMS provides real-time measurements of ensemble-averaged properties for submicron non-refractory aerosol, it does not achieve molecular speciation and thus

cannot be used to identify individual compounds present in OA. Typical AMS BBOA studies use *m/z* 60 ($C_2H_4O_2^+$) and *m/z* 44 (CO_2^+) signals to quantify primary and aged emissions, respectively (e.g. Cubison et al., 2011; Ng et al., 2010, 2011). Levoglucosan, a cellulose decomposition product often used as a molecular tracer for freshly-emitted BBOA (e.g. Simoneit et al., 1999, 2004), is frequently considered to be a primary contributor to *m/z* 60 in AMS laboratory and field studies (e.g. Lee et al., 2010; Ng et al., 2011b). However, while levoglucosan has traditionally been understood to remain stable over relevant timescales (Fraser and Lakshmanan, 2000; Locker, 1988; Simoneit et al., 1999), multiple laboratory studies suggest that hydroxyl radical (OH·)-driven levoglucosan decay occurs at a timescale similar to transport and deposition timescales (Hennigan et al., 2010; Hoffmann et al., 2010; Lai et al., 2014). Additionally, recent measurements demonstrate that *m/z* 60 abundances may remain above background levels with sufficient atmospheric processing, suggesting that not all *m/z* 60 originates from BBOA (Cubison et al., 2011; Ortega et al., 2013). These two considerations highlight the need for *in situ* molecular speciation measurements to complement bulk aerosol chemical data supplied by the AMS.

The Thermal desorption Aerosol Gas chromatograph (TAG) pairs automated aerosol collection and thermal desorption with gas chromatography-mass spectrometry (GC-MS), providing molecular level speciation with *in situ* analysis and hourly time resolution (Williams et al., 2006). The TAG has been used in field studies to identify molecular tracers in ambient air and to link different chemical profiles to unique sources (e.g. Kreisberg et al., 2009; Lambe et al., 2009; Williams et al., 2007, 2010, 2014; Worton et al., 2011; Zhang et al., 2014, 2016). The TAG is capable of providing speciated compound measurements for approximately 20% of total organic aerosol mass on average, depending on the type of aerosol collected (Williams et al., 2006). While the TAG reliably detects a high fraction (up to 100%) of hydrocarbon OA mass, which is typical of POA, the analyzed fraction of oxidized OA mass is often much lower (Williams et al., 2010, 2016; Zhang et al., 2014). This discrepancy is attributed to low mass throughput of oxidized species through the 30 m non-polar GC capillary column (Williams et al., 2006, 2016) and presents a disadvantage for TAG analysis of oxidized components typical of SOA.

Recent advances have expanded the TAG's analytical capability. Traditional gas chromatography utilizes a solvent delay to prevent detector damage from large solvent or water signals. In the TAG, much of the solvent can be purged prior to sample injection, and the solvent delay is no longer applied. The lack of a solvent delay allows volatile components and aerosol thermal decomposition products to reach the detector during thermal sample desorption (5-15 minutes of TAG GC program) from the TAG collection cell to the GC column. The mass-spectral signal within this period, called the thermal decomposition window, typically features an air signal (e.g., *m/z* 32 for O_2^+, *m/z* 40 for Ar^+, *m/z* 44 for CO_2^+), but can also contain ions characteristic of decomposing nitrates (*m/z* 30 for NO^+, *m/z* 46 for NO_2^+), sulfates (*m/z* 48 for SO^+, *m/z* 64 for SO_2^+), and organics (*m/z* 44 for CO_2^+). These ion signals were shown to correlate with corresponding AMS ions for ambient data collected during the Saint Louis Air Quality Regional Study in 2013 (Williams et al., 2016). However, because the TAG thermal decomposition window has only recently been used to analyze ambient data, more laboratory studies are needed to explore the thermal decomposition products of OA from unique sources.

In this work, we present results from laboratory studies aimed at characterizing BBOA chemical composition using both the TAG compound window (minutes 20-55 of the chromatogram; Figure 1) and the TAG thermal decomposition window (minutes 6-16 of the chromatogram; Figure 1) in parallel with an AMS. A custom-built emissions and combustion chamber was used to generate BBOA, and a Potential Aerosol Mass (PAM) oxidative flow reactor (OFR), which can mimic up to 16 days of atmospheric aging with residence times on the order of 100 seconds (Kang et al., 2007; Lambe et al., 2011), was used to oxidize laboratory-generated BBOA plumes at different levels of accelerated photochemistry. Our experiments addressed three primary objectives. First, the chemical composition of laboratory-generated BBOA was explored to identify molecular tracers from the leaf and heartwood of the American white oak (*Quercus alba*). Recently developed chromatogram-binning Positive Matrix Factorization (PMF) techniques (Zhang et al., 2014, 2016) were applied to the TAG compound window to determine the prevalence of different compound classes and functionalities unique to BBOA from each fuel type. Trends in compounds and compound classes of interest with oxidation were evaluated using both individual compound integrations and chromatogram binning PMF results. Second, the TAG thermal decomposition window was used to investigate how the chemical composition of thermally decomposing BBOA varies with PAM aging. Concurrent AMS measurements were taken to complement TAG decomposition window data, providing $\overline{OS_C}$ estimations and high-resolution ion signals for bulk BBOA samples. These AMS parameters were used to inform interpretation of TAG decomposition ion signals, particularly the variation of TAG decomposition *m/z* 44 and *m/z* 60 signals with extent of oxidation in the PAM chamber. Additionally, chromatogram-binning PMF techniques (Zhang et al., 2014, 2016) were applied to the decomposition window to investigate the presence and covariance of key ion signals. Finally, trends in TAG and AMS *m/z* 60 signals with PAM aging were explored to evaluate the utility of *m/z* 60 as a tracer for freshly-emitted BBOA. We present evidence that, depending on biomass source and atmospheric conditions, a significant fraction of AMS *m/z* 60, which is typically used to track primary BBOA in the atmosphere, may be attributed to aged OA mass.

2 Materials and Methods

2.1 Emissions and Combustion Chamber

A flow diagram of the experimental setup and a diagram of the custom-built emissions and combustion chamber are given in Supplemental Information (Figures S1 and S2, respectively). The chamber is a rectangular 1.48 m^3 chamber made of ¼" thick tempered glass panels secured by aluminum framing (80/20, Inc., Columbia City, IN). The chamber is divided into two compartments, separated by a sheet of aluminum serving as a baffle with a central hole 3 cm in diameter. In the first compartment, biomass samples are resistively heated in PID-controlled stainless steel cups installed along the chamber floor. The second compartment serves as a mixing chamber from which primary gases and particles are sampled at 10 L min^{-1}. Air was treated with a HEPA filter (Pall Corporation, Port Washington, NY) and a hydrocarbon trap (Model BHT-4, Agilent Technologies, Santa Clara, CA), then supplied to the heating compartment of the chamber to promote consistent mixing. Both compartments are extensively vented between experiments to clear the chamber of gases and particles.

2.2 Devolatilization and Combustion Experiments

The white oak biomass samples used in this study were collected at the Tyson Research Center in Eureka, MO, located approximately 20 miles outside of St. Louis, MO. An oak trunk segment was taken from the site, and heartwood samples were collected by drilling into the center of the trunk segment. Oak leaves were clipped from a single branch that was taken directly from a live tree. The leaf samples were air-dried for at least one week and milled into fine pieces using a tobacco grinder prior to running the experiment. All biomass was stored at room temperature (20-25°C), and moisture content was not controlled for either fuel type.

Samples of oak wood or leaf were pre-weighed (0.2-0.5 g), placed in the emissions chamber cup, and spread evenly across the bottom rim. The cup was heated for 3.5 minutes, with temperatures in the cup reaching a maximum of 215°C. In this work, we use the term "devolatilization" to describe the non-combustive release of emissions from biomass fuels at elevated temperatures. During the heat pulse, the biomass sample was first devolatilized, with smoldering embers observed in the final minute of the heat ramp. To ensure the TAG and AMS collected particles within a similar size range, primary emissions were passed through a PM_1 cyclone (Thermo Fischer Scientific, Waltham, MA) operated at 16.7 L min^{-1} to remove particles too large to be sampled by the AMS (DeCarlo et al., 2006).

Because dilution is known to drive partitioning of SVOCs and IVOCs from the particle phase into the gas phase in BBOA plumes (Grieshop et al., 2009; Ortega et al., 2013), dilution was minimized in the system during devolatilization and combustion experiments. Dilution air, purified using separate zero air generators (Model 737, Aadco Instruments, Cleves, OH), was supplied before the PM_1 cyclone (6.7 L min^{-1}) and after the PAM chamber (4 L min^{-1}) to provide sufficient flow to the cyclone and to all instruments (Figure S1), giving a net dilution ratio of approximately 5 for all experiments.

2.3 PAM Reactor Operation

Particulate and gas-phase emissions were treated together in the PAM flow reactor. A detailed description of the PAM reactor is given elsewhere (Kang et. al. 2007, Lambe et. al. 2011). The reactor consists of a 13 L cylindrical aluminum chamber coated internally with Iridite 14-2 (MacDermid, Inc., Waterbury, CT), a chromate conversion film applied to inhibit wall losses. Within the PAM chamber, low-pressure mercury lamps emit light at two wavelengths (185 nm and 254 nm) in the UV range, and different OH· concentrations are produced by adjusting the intensity of the UV irradiation (Kang et al., 2007). Ozone (O_3) is produced externally by irradiating 0.4 L min^{-1} of pure O_2 with mercury lamps (λ = 185 nm; BHK, Inc., Ontario, CA). Water vapor is introduced into the PAM reactor with 4.6 L min^{-1} of humidified N_2. A total flow rate of 10 L min^{-1} was maintained throughout the experiments, giving an average residence time of 78 seconds within the reactor. To achieve consistent OH· formation, the relative humidity (RH) inside of the reactor was kept at 30.0% ± 3.7% (one standard deviation), measured with a relative humidity and temperature probe with manufacturer-specified accuracy of 1.5% (Vaisala, Inc., Woburn, MA). RH was altered by controlling N_2 flow through a Nafion membrane humidifier (Perma Pure LLC, Lakewood, NJ). The role of RH in OH· formation is discussed in detail in Supplemental Information (Method: PAM Calibrations and Figure S3).

OH· exposures (OH_{exp}) within the PAM reactor were calculated using the offline sulfur dioxide (SO_2) calibration method described in previous work (Kang et al., 2007). During reactor calibration, SO_2 concentrations (Airgas, Inc., Radnor, PA) were measured with an SO_2 monitor (Model 43i-TLE analyzer, Thermo Fischer Scientific, Waltham, MA) at varied UV lamp intensities; similarly, O_3 was measured downstream of the PAM reactor by UV photometry (Model 49i, Thermo Fischer Scientific, Waltham, MA). Equivalent atmospheric aging times (Table 1) were calculated assuming an average atmospheric OH· concentration of 1.5×10^6 molec cm^{-3} (Mao et al., 2009). PAM reactor calibration details and results are provided in Supplemental Information (Method: PAM Calibrations). For both heartwood and leaf, experiments were performed at two level of photochemical aging in addition to a baseline without exposure. Henceforward, the different photochemical aging conditions will be denoted by the corresponding equivalent aging time (Table 1).

Previous PAM reactor studies have demonstrated that high concentrations of volatile organic compounds (VOCs) can suppress OH· reactivity (Li et al., 2015; Peng et al., 2015). This suppression occurs because VOCs drive rapid conversion of OH· to HO_2, and recycling of HO_2 back to OH· can be slow without addition of sufficient O_3 (Peng et al., 2015). The external production of O_3 featured in our system is expected to reduce OH· suppression by introducing additional O_3 to promote recycling of HO_2 back to OH· (Peng et al., 2015). However, because the reactor was calibrated offline without additional injection of VOCs, obtaining OH_{exp} values characteristic of the experimental setup remains challenging (Ortega et al., 2013). Based on an RH of 30% and a typical output O_3 range of 4.3-8.5 ppm (measured during reactor calibrations), we estimated OH_{exp} ranges for each PAM UV light setting using the Oxidation Flow Reactor Exposure Estimator version 2.3 developed by Peng, et al., available for download at http://sites.google.com/site/pamwiki/hardware/estimation-equations (Peng et al., 2015). Results obtained using this spreadsheet are provided in Supplemental Information (Table S1). The "condition type," which indicates whether VOC suppression is significant under the input conditions, was found to be largely dependent on the assumed external OH· reactivity (OHR_{ext}), which is difficult to assess without direct VOC measurements.

2.4 Instrumentation and Data Analysis

The TAG and the AMS were used to collect complementary chemical composition data. A Scanning Mobility Particle Sizer (SMPS; Model 3081 DMA, Model 3022A CPC, TSI, Inc., Shoreview, MN) was used to measure aerosol size distributions and volume concentrations.

The devolatilization and combustion experiments were performed in two distinct experimentation periods. In the first period, the procedure was done at each level of PAM oxidation using 0.2 g biomass. Triplicate experiments were done with the TAG and the SMPS during this period to ensure repeatability of the devolatilization and combustion cycle. In the second experimentation period, experiments were performed once more at each level of oxidation to obtain simultaneous TAG, SMPS, and AMS measurements. For these experiments, the devolatilization and combustion procedure was done with more biomass (0.5 g) so the AMS could obtain sufficient signal.

2.4.1 Thermal Desorption Aerosol Gas Chromatograph (TAG)

A full description of the TAG system is provided elsewhere (Williams et al., 2006). Particles are collected via humidification and inertial impaction at a typical flow rate of 9.3 L min^{-1}, with a particle cutoff (d_{p50}) of approximately 70 nm (Williams et al., 2006). Following sample collection, the collection and thermal desorption (CTD) cell is heated to 310 ºC to thermally desorb the collected OA. The desorbed sample is flushed through a heated transfer line using helium as an inert carrier gas and transported to a gas chromatography column for separation and mass spectral detection. An Agilent 6890 gas chromatograph (Agilent Technologies, Santa Clara, CA) with a 30m-long 0.25mm i.d. RTX5-MS non-polar fused silica capillary column (Restek Corporation, Bellefonte, PA) was used to achieve chromatographic separation. A 70 eV electron ionization quadrupole mass spectrometer (5973 MSD, Agilent Technologies, Santa Clara, CA), operated to scan between 29-450 *m/z*, provided mass spectral detection. TAG performance was evaluated regularly (once every 1-3 days) using 5 ng C_{12}-C_{40} even alkane standard mixture (Sigma Aldrich, St. Louis, MO) manually injected onto the CTD cell and thermally desorbed onto the GC column via a helium carrier stream (Kreisberg et al., 2009).

TAG data was collected during the first experimentation period using 0.2 g biomass in the heat pulse. For all the oak leaf and oak wood experiments, particles were collected on the TAG for four minutes, thirty minutes after the heat pulse was performed in the emissions chamber. The TAG collected two additional samples over the course of three hours to ensure that the emissions and combustion chamber was clean prior to the subsequent devolatilization cycle.

In this work, the TAG compound and thermal decomposition time windows were analyzed as complementary sets of chemical data (Figure 1). As defined for this study, the thermal decomposition window occurs between minutes 6-16 of GC analysis, which coincides with the thermal desorption of sample from the CTD cell. The compound window consists of material eluting from minutes 20-55 of analysis following condensation of desorbed sample at the column head. This window contains information on OA components that have been successfully desorbed, transferred, and separated.

Prior to each experiment, a system blank chromatogram was obtained by sampling from the empty emissions chamber through the PAM reactor, with the PAM UV lamps set to the voltage corresponding to the subsequent equivalent aging time to be tested. A system blank was subtracted from each chromatogram prior to data processing to correct for both TAG system artifacts (e.g. air signal and column bleed) and sampling system (PAM reactor and emissions and combustion chamber) artifacts. Additionally, to isolate changes in aerosol chemical properties from changes in aerosol mass with photochemical aging, each blank-subtracted chromatogram was normalized to volume concentration by dividing the abundance at each scan by the maximum volume concentration (μm^3 cm^{-3}) obtained by the SMPS for each devolatilization cycle (Table S2 and Figure S4 in Supplemental Information). This blank subtraction and normalization process was done for all total ion count (TIC) chromatograms and single-ion chromatograms (SICs) presented in this work.

2.4.2 TAG Positive Matrix Factorization

Positive matrix factorization (PMF) was performed on TAG chromatograms to identify source-specific major compounds and compound classes present in the oak wood and leaf BBOA. TAG chromatograms were binned by

retention time according to the method outlined in previous work (Zhang et al., 2014, 2016). Prior to chromatogram binning, each chromatogram was blank-subtracted to minimize the contribution of background noise in PMF calculations. An instrument error of 10%, chosen based on a typical average TAG instrument error of 10% (Williams et al., 2006), was assumed during PMF calculations.

The GC-resolved mass spectral PMF method for binned TAG data was developed to separate compounds in TAG chromatograms into chemically similar factors, improving analysis efficiency (Zhang et al., 2014). With this method, mass spectral data is supplied to the PMF model, and solutions are obtained using the PMF2 algorithm (Paatero, 1997). Each resulting factor consists of a mass spectrum corresponding to a compound or class of compounds present in the TAG chromatograms (Zhang et al., 2014). This PMF method was performed on the compound and decomposition analytical windows separately for data obtained from both BBOA sources. PMF output and solutions were evaluated using custom-built pre- and post-processing analysis software in conjunction with the PMF Evaluation Tool (version 3.00A; Ulbrich et al., 2009) in Igor Pro version 6.38Beta01 (WaveMetrics, Inc.). Mass spectral identification of different factors was aided by the NIST MS Search Program version 2.0, available for download at http://chemdata.nist.gov/mass-spc/ms-search/.

The number of appropriate PMF factors was determined for each solution based on two considerations. First, in a typical PMF analysis, the optimal number of factors in a solution is selected based on the objective function Q, which is the sum of weighed squared residuals (Paatero, 1997). The Q/Q_{exp} value, or the ratio of the actual objective function to the expected objective function assuming normally distributed residuals, should ideally approach 1; too few factors may result in a large Q/Q_{exp}, indicating that errors have been underestimated in PMF calculations (Ulbrich et al., 2009). Additionally, if too many factors are specified, the solution may feature split factors, where information from a compound or compound class is distributed across multiple factors. In this work, the number of factors presented for each analysis was selected to minimize split factors while maximizing identifiable factors. Because of the TAG data's high chromatographic resolution, low rotational ambiguity was assumed, and all calculations were performed with $f_{peak} = 0$. This assumption is supported by previous work, where TAG data was not sensitive to f_{peak} or starting point (seeds) during PMF analysis (Williams et al., 2010).

2.4.3 AMS

The AMS data presented in this work were obtained using 0.5 g of biomass in the heat pulse instead of 0.2 g to ensure the AMS received sufficient signal. The AMS was operated in V-mode throughout all experiments (DeCarlo et al., 2006). AMS data was processed in Igor Pro version 6.38Beta01 using the SQUIRREL version 1.57 toolkit for unit mass resolution analysis and the PIKA version 1.16 toolkit for high resolution analysis. Both AMS data analysis tools are available for download at http://cires1.colorado.edu/jimenez-group/ToFAMSResources/ToFSoftware/index.html.

3 Results and Discussion

3.1 Individual Compound Analysis

For both leaf and wood BBOA, key molecules identified within the compound window of the TAG chromatograms are given in Supplemental Information (Tables S3 and S4). Corresponding molecular structures for the compounds used in individual compound analysis are also provided (Figures S5 and S6). Identification certainty ("Certainty of ID") was classified for each compound according to the following criteria: A) the compound was positively identified based on external standard injections; B) the compound was identified based on a high match quality (MQ > 75%) using available mass spectral libraries; C) the compound was identified based on a low-to-moderate match quality (50% < MQ < 75%) using available mass spectral libraries; and D) no adequate mass spectral library match was available for the compound, so the compound structure was determined by retention time and manually evaluating possible fragmentation patterns. Subcooled liquid vapor pressures at 25°C were predicted for each compound using the Advanced Chemistry Development (ACD/Labs) Software V11.02 (© 1994-2017 ACD/Labs), available for use on the SciFinder website (ACD/Labs, 2017).

3.1.1 Trends in Individual Compounds with Photochemical Aging

Leaf and wood BBOA chromatograms at three levels of photochemical aging are overlaid for comparison in Figure 2. Raw peak integration values with standard deviations are provided for each compound at each level of equivalent aging are also provided (Tables S5 and S6 in Supplemental Information). Each plot constitutes an average of triplicate blank-subtracted measurements, with each chromatogram normalized to the maximum total volume concentration measured during the experiment as described previously. For these plots, the averaged, normalized chromatograms at each level of aging were further normalized to the point of highest abundance in the unaged ("0 days") average chromatogram. In the leaf BBOA chromatograms (Figure 2a), many of the low volatility species eluting after minute 35 of the GC analysis are long-chain alkanes, alcohols, aldehydes, and terpenoids, compounds commonly found in the leaf's waxy exterior coating (Gulz and Boor, 1992). Based on even-numbered alkane standard injections, compounds eluting after minute 35 exhibit approximate saturation vapor pressures not exceeding 2.73×10^{-5} torr at 25ºC (Table S3 in Supplemental Information; ACD/Labs, 2017). Nearly all compounds identified after 35 minutes decrease in abundance with photochemical aging. To illustrate the relative rates of decay that each compound experiences in the PAM reactor, Figure 3a provides integrated abundances, first normalized to appropriate volume concentrations then to corresponding abundances at no oxidation, for nine compounds of interest. Notably, we have identified an even-carbon aliphatic aldehyde series based on $[M-18]^+$ and $[M-28]^+$ (where M is the parent mass) peaks present in the mass spectra of each of the compounds (Watson and Sparkman, 2007). As the carbon number (n_C) increases, the aldehyde abundance decreases more readily with oxidation. To our knowledge, rate constants for the reaction of long-chain ($n_C \geq C_{20}$+) aliphatic aldehydes with OH· have not been reported. However, previous studies on short-chain ($n_C \leq C_{14}$) aliphatic aldehydes demonstrate that OH· reaction rate constant increases with increasing carbon chain length (D'Anna et al., 2001; Niki et al., 1978). Although aliphatic aldehydes, particularly C_{26} and C_{28} aldehydes, have been characterized as components of oak leaf waxes (Gulz and Boor, 1992), this series of aldehydes has not been previously reported as components of oak leaf BBOA and may therefore serve as novel tracer species in future field experiments. Solvent extractions performed on oak leaves using TAG CTD injections confirm that the

aldehydes are present in the leaf wax prior to devolatilization and combustion (Method: Oak Leaf Solvent Extractions and Figure S7 in Supplemental Information).

Compounds characteristic of wood primary BBOA are typically more volatile than those found in the leaf primary BBOA, eluting between minutes 28 and 35 of the GC analysis (Figure 2b). Based on even alkane standard injections, compounds eluting within this time window exhibit approximate vapor pressures within 4.52×10^{-3}-2.73×10^{-5} torr at 25ºC (Table S4 in Supplemental Information; ACD/Labs, 2017). The compound with the highest abundance in unoxidized wood BBOA chromatograms is sinapaldehyde (4-hydroxy-3,5-dimethoxycinnamaldehyde), a phenolic compound derived from lignin. Sinapaldehyde reacts rapidly in the PAM reactor, with the normalized average integrated peak area decreasing by approximately 70% from 0 days to 3.4 days of equivalent aging (Figure 3b). Other compounds, including guanosine, galactoheptulose, and acetylgalactosamine, also exhibit decreases in abundance; relative rates of decay for these and other wood BBOA tracers are given in Figure 3b.

Syringol (2,6-dimethoxy-phenol), syringaldehyde (4-hydroxy-3,5-dimethoxy-benzaldehyde), and vanillin (4-hydroxy-3-methoxy-benzaldehyde) increase in abundance from 0 days to 3.4 days of equivalent aging and are fully depleted with 9.8 days of equivalent aging. Since the average volume concentration for runs at 3.4 days of aging were larger than those at 0 days of aging by a factor of approximately 1.3 (Table S2 in Supplemental Information), the factor of ~2 increase in syringol and syringaldehyde integrated abundances could occur due to partitioning from the gas phase into the particle phase. However, the nearly eight-fold increase in vanillin integrated abundance from 0 days to 3.4 days of aging suggests an alternative formation mechanism driven by reactions occurring in the PAM reactor. One potential mechanism for the formation of aldehydes from larger lignin decomposition products, described in Supplemental Information (Figure S8), involves the cleavage of the C_α-C_β unsaturated bond on the benzyl substituent following abstraction of the hydrogen from the phenolic substituent group. A mechanism for vanillin formation from larger lignin decomposition products has been previously described as part of an alkaline oxygen delignification process and involves the formation and fragmentation of a peroxide radical intermediate (Wong et al., 2010). The presence of OH· in the PAM reactor may drive a similar process, leading to increases in vanillin abundance at moderate OH_{exp}.

3.1.2 Compound Window PMF Analysis

GC-MS PMF results are provided for both leaf and wood BBOA chromatograms using data collected within the TAG compound window (Figures 4, 5, 6, and 7). Q/Q_{exp} and residual plots are provided in Supplemental Information (Figures S9 and S10, respectively). The chromatograms (Figures 4 and 6) are displayed as averages of binned data from triplicate measurements at each level of oxidation and are displayed in one trace; different equivalent aging times are demarcated with vertical lines along the x-axis. Corresponding mass spectra (Figures 5 and 7) are identified and displayed with key ions labeled. High factor solutions (≥15) were used for compound window data to best deconvolve the large and complex mixture of compounds. However, in some cases, factor splitting resulted in the distribution of ions between two or more factors, made evident by similarities retention times. Wherever possible, split factors were recombined by summing the binned chromatograms and the mass spectra and are labeled accordingly (e.g. “F10+F12”

indicates that factor 10 and factor 12 have been recombined). In general, for the compound window, factor solutions were chosen to maximize the number of identifiable factors while minimizing the number of split factors.

A 15-factor solution was chosen to deconvolve leaf BBOA compound window chromatograms (Figures 4 and 5; additional information provided in Figures S9a and S10a). This solution provided enough factors to resolve the lowest-abundance components (e.g. F1), and increasing the number of factors past 15 led to greater factor splitting without providing additional insight into the chromatograms. Among the factors identifiable with this solution include quinic acid (Factor 2, F2), sugars and anhydrosugars (e.g. mannose; F3), alcohols and alkenes (F6), aldehydes (F10), terpenoids (e.g. friedelin; F11), and column bleed (F13+F14). Other factors (F1, F5+F7, F9+F12, F15) correspond to different classes of unresolved complex mixture (UCM) and have been tentatively identified by considering the closest matches in the NIST mass spectral database. Factor 4 (F4) is identified as a split factor, exhibiting mass spectral characteristics of multiple factors, including acids (*m/z* 129) and anhydrosugars (*m/z* 116). Factors 13 and 14 demonstrate contributions from both terpenoid-like UCM and column bleed and are therefore combined. The presence of alkylbenzenes (F8), dominated by *m/z* 91 ($C_7H_7^+$) and *m/z* 92 ($C_7H_8^+$), is noteworthy, as alkylbenzenes are typical of anthropogenic materials (e.g. detergent precursors produced from petroleum; Forman et al., 2014) and have not been reported as components of biomass. Since the leaves were not cleaned after they were collected, the alkylbenzenes could come from deposition of fuel combustion aerosol onto the leaves' surface prior to biomass sample collection. The presence of alkylbenzenes on the surface of the leaf was confirmed with TAG analysis of solvent-extracted leaf surface components (Figure S11), supporting the interpretation of deposition of anthropogenic compounds on the leaf's exterior.

An 18-factor solution was applied to deconvolve compounds in the wood BBOA chromatograms (Figures 6, 7; additional information provided in Figures S9b and S10b). Notable factors correspond to levoglucosan (F1), guaiacol (F4), vanillin and guaiacyl compounds (F7), syringol (F8), syringaldehyde (F10), sinapaldehyde (F11), and column bleed (F18). Based on retention time and mass spectral characteristics (e.g. *m/z* 77), factor 5 (F5) corresponds to aromatic species and is not matched to a single compound. Factor 6 (F6) is featured in multiple aromatic compounds, but is also present in levoglucosan in very low abundances. Several types of UCM (F2, F3, F9, F12+F13+F14, F15, F16) were deconvolved and tentatively identified using the top matches from the mass spectral database. Factor 16 (F16) is predominated by siloxanes (e.g. *m/z* 73, *m/z* 281, *m/z* 341), though some UCM has been split from other factors. Finally, factor 17 (F17) exhibits characteristics of multiple classes of compounds and is therefore identified as a split factor.

Nearly all factors obtained in the leaf BBOA compound window analysis decrease with photochemical aging, including quinic acid (F2), sugars and anhydrosugars (F3), alkanes and long-chain aliphatics (F6, F10, F15), alkylbenzenes (F8), terpenoid components (F11), and various classes of UCM (F1, F4, F5+F7, F9+F12). This trend agrees well with the individual compound results and further indicate that primary components undergo increased fragmentation at higher OH_{exp}. In the wood BBOA, some primary components decrease steadily with photochemical aging, including sinapaldehyde (F11), aromatics (F5), and various classes of UCM (F12+F13+F14, F15, F17). Other factors, including guaiacol (F4), vanillin (F7), syringol (F8), and syringaldehyde, exhibit a strong increase in

abundance at 3.4 days of aging followed by a decrease at 9.8 days of aging, possibly due to changes in partitioning as described previously. Levoglucosan (F1) also appears to increase slightly in abundance at 3.4 days of equivalent aging, though this is likely due to differences in aerosol mass produced between experiments. Results from both types of BBOA show changes in column bleed (F13+14 and F18 for leaf and wood BBOA, respectively) from unaged chromatograms to 9.8 days of aging. While the column bleed decreases with photochemical aging in both cases, this trend is due to differences in blank subtractions from run to run and is not related to changes in photochemical aging.

The PMF deconvolution results support the identification and analysis of individual tracers present in wood and leaf BBOA. Because each chromatogram may contain hundreds of individual compounds, a general knowledge of the compound classes characteristic of each BBOA type can greatly reduce individual compound analysis time and ensure that chromatograms are characterized as completely as possible. The results presented in this study therefore confirm that the chromatogram binning method coupled with PMF, as developed by Zhang, et al. (Zhang et al., 2014, 2016), can aid molecular tracer analysis by elucidating different compound classes of interest present in BBOA. The PMF results obtained in this study for the compound window provide information on characteristic mass spectral signatures within leaf and wood primary BBOA and may be compared to results obtained in future BBOA studies to more fully characterize how different compounds evolve with photochemical aging in the atmosphere.

3.2 TAG Thermal Decomposition Window

The thermal decomposition window has been used in previous work to assess contributions of inorganic (nitrates, sulfates, etc.) and organic species present in atmospheric aerosol (Williams et al., 2016). In this work, we provide evidence that the TAG thermal decomposition window can be used to evaluate the relative level of oxidation of bulk OA samples using the *m/z* 44 (CO_2^+) ion. In addition, we demonstrate that other fragments within the decomposition window may give insight into the chemical composition of aged, thermally labile BBOA.

Replicable, quantitative TAG data were not obtained during experiments that used 0.5 g biomass, potentially due to a minor system leak. However, the TAG chromatograms that were obtained using 0.5 g biomass were chemically similar to the triplicate TAG chromatograms obtained using 0.2 g biomass, and we therefore compare all AMS data with TAG chromatograms collected using 0.2 g biomass in subsequent analysis. Chemical similarity between chromatograms was confirmed using the dot product mass spectral comparison method outlined by Stein and Scott (Stein and Scott, 1994). For each blank-subtracted TAG chromatogram, a summed mass spectrum was obtained by summing all ions (*m/z* 33-*m/z* 450) across all scans (retention times) in the chromatogram and converting the resulting mass spectral vector into a unit vector. To assess the similarity of two mass spectra, the dot product of the mass spectral unit vectors was calculated; a dot product of 1 signifies a perfect mass spectral match, and a dot product of 0 indicates a complete mismatch (Stein and Scott, 1994). In this work, the dot product was determined for two chromatograms, one obtained with 0.5 g biomass and one obtained with 0.2 g biomass, at each level of oxidation. The resulting dot products for both leaf and wood oak are all above 0.75 and are provided in Supplemental Information (Figure S12; Table S7).

3.2.1 *m/z* 44 as a Tracer for Aged OA

Figures 8a and 8b show *m/z* 44 TAG decomposition SICs for leaf and wood BBOA, respectively. The displayed SICs have each been blank subtracted, normalized to maximum volume concentrations, and averaged across triplicate measurements at each level of oxidation. Within each plot, the chromatograms have been further normalized to the point of highest abundance within the unaged ("0 days") *m/z* 44 signal. The *m/z* 44 signals were also summed across the entire decomposition window following blank subtraction, normalization to appropriate volume concentrations, and triplicate averaging, and are provided as functions of equivalent aging time (± one standard deviation) in Figure 8c. The upward trend in the *m/z* 44 signal between minutes 6 and 10 of GC analysis coincides with the CTD temperature ramp from 45°C to 310°C, and is thus consistent with gradual increase in OA thermal decomposition as the temperature rises. The subsequent decrease in *m/z* 44 signal from minute 10-16 reflects the thermal decomposition of remaining material as the CTD cell is held at 310°C. For both types of BBOA, the decomposition *m/z* 44 integrated signal increases overall from 0 days to 9.8 days of equivalent aging, indicating that OA thermal decomposition increases overall with increased PAM oxidation. This trend is consistent with increased formation of more highly oxidized aerosol within the PAM reactor. In the leaf BBOA chromatograms, the increase in integrated *m/z* 44 signal is most pronounced from 0 to 3.4 days of equivalent aging, while the wood BBOA data exhibits the most dramatic increase from 3.4 to 9.8 days. The variation in the shape of the decomposition *m/z* signal between the two types of biomass likely reflects differences in thermal lability between different types of OA.

AMS $\overline{OS_C}$ values calculated for both types of biomass range from -1.5 to -0.2 (Figure 9). In both types of BBOA, an increase in relative integrated TAG decomposition *m/z* 44 signal coincides with an increase in $\overline{OS_C}$ from 0 to 9.8 days of photochemical aging. A linear correlation between decomposition *m/z* 44 and AMS $\overline{OS_C}$ for wood BBOA (r^2 = 0.9986) indicates that under these experimental conditions, the TAG thermal decomposition window has the potential to provide quantitative measurements of bulk OA oxidation levels. By contrast, leaf BBOA decomposition *m/z* 44 and AMS $\overline{OS_C}$ correlate poorly (r^2 = 0.7842 for a linear fit). The non-linear trend in TAG decomposition *m/z* 44 for leaf BBOA may indicate a shift in the dominant oxidation mechanisms between moderate and high levels of OH· within the PAM chamber; at the highest OH_{exp}, primary gas and/or particle-phase components may undergo increased fragmentation, leading to a net decrease in production of the aged OA that thermally decomposes during TAG analysis. However, the mechanisms behind this trend remain unclear and merit further investigation.

For each fuel type, AMS f_{44} vs f_{43} data have been plotted at each level of equivalent aging (Figure 10). To further explore the TAG's analytical capability in relation to AMS bulk chemical data, TAG integrated ion fractions (f_{ion}) are provided on the plots. These fractions are defined as the blank-subtracted integrated ion signal divided by the blank-subtracted integrated TIC signal. For example, for a chromatogram *i*, the TAG f_{44} signal is defined as:

$$f_{44,i} = \frac{(A_{44})_i - (A_{44})_{blank}}{(A_{TIC})_i - (A_{TIC})_{blank}} \quad (1)$$

where $(A_{44})_i$ is the integrated *m/z* 44 signal across all (i.e., TAG total chromatogram) or part (i.e., TAG compound window) of *i*, $(A_{44})_{blank}$ is the integrated *m/z* 44 signal across a blank chromatogram, $(A_{TIC})_i$ is the integrated TIC across all or part of *i*, and $(A_{TIC})_{blank}$ is the integrated TIC across the same blank. For wood BBOA, while AMS f_{44} increases and f_{43} decreases with photochemical aging, both TAG f_{44} and f_{43} increase with increasing oxidation, particularly when

the decomposition window is included in analysis (i.e., TAG total chromatogram). However, TAG fractions from the leaf BBOA data are more varied and do not exhibit a clear trend. In general, the TAG fractions tend to fall to the left of AMS f_{44} vs f_{43} data points, indicating that the TAG excels at throughput of less-oxygenated hydrocarbon OA. However, the increase in TAG f_{44} with inclusion of decomposition window material shows a clearer oxidation trend that is in greater agreement with the AMS oxidation trend.

3.2.2 Decomposition Window PMF Analysis

To aid identification of key thermal decomposition products, the binning deconvolution PMF method was applied to the TAG chromatogram decomposition window (Figures 11, 12, 13, 14). Details of the PMF analyses are provided in Supplemental Information (Figures S9 and S10). Tentative identification of different factors was facilitated by the NIST mass spectral database, though standard injections are needed to adequately quantify the decomposition window signal and identify the factors with complete confidence. As with the compound window PMF results, chromatograms are displayed as triplicate averages of binned data at each level of oxidation and are demarcated by vertical lines across the x-axis (Figures 11, 13). Key ions are labeled and tentative identifications are provided above each mass spectrum (Figure 12, 14).

For the leaf BBOA chromatograms, a 4-factor solution gave several distinguishable factors (Figures 11, 12; additional information provided in Figures S9c and S9c), including the *m/z* 44 (CO_2^+) signal previously identified as originating from thermal decomposition oxidized organics (F1). Factor 3 (F3), dominated by *m/z* 78 (possibly $C_6H_6^+$) with smaller contributions from *m/z* 39 ($C_3H_3^+$) and *m/z* 51 ($C_4H_3^+$), could indicate decomposing aromatics. Factor 2 (F2) matches with nitrogenated compounds in the mass spectral database, and the co-elution of *m/z* 43 (possibly $C_2H_3O^+$) and *m/z* 79 (possibly $C_4H_3N_2O^+$) could signal the presence of nitrogenated oxidized organics. Finally, factor 4 (F4) is dominated by multiple fragments characteristic of less-oxidized or unsaturated organic material, including *m/z* 55 ($C_4H_7^+$), *m/z* 67 ($C_5H_7^+$), and *m/z* 91 ($C_7H_7^+$); this factor may also include contributions from air (*m/z* 40; Ar^+) and *m/z* 79 split from factor 3.

A 5-factor solution was chosen for the wood BBOA chromatograms (Figures 13, 14; additional information provided in Figures S9d and S9d). Factor 1 (F1) is dominated by *m/z* 44, attributed to decomposing oxidized organics (CO_2^+). Acetic acid was identifiable in factor 2 (F2) based on relative abundances of *m/z* 43 ($C_2H_3O^+$), *m/z* 45 (CHO_2^+), and *m/z* 60 ($C_2H_4O_2^+$), suggesting that organic acids comprise part of the thermal decomposition OA. Factor 3 (F3) features *m/z* 50 and *m/z* 52 (possibly $CH_3{}^{35}Cl^+$ and $CH_3{}^{37}Cl^+$, respectively) in the 3:1 isotopic ratio characteristic of chlorine, indicating that the wood BBOA may contain chlorinated organics. Based on comparison of retention times, the large contribution of *m/z* 44 to factor 3 may be due to splitting from factor 1. Factor 4 is dominated by ions characteristic of less-oxygenated or unsaturated organic material, including *m/z* 55 ($C_4H_7^+$), *m/z* 72 ($C_4H_8O^+$), and *m/z* 84 ($C_5H_8O^+$). Lastly, factor 5 (F5) has been identified as furfural using the mass spectral database, which has been previously reported in gas-phase mass spectral measurements of biomass burning emissions (Stockwell et al., 2015).

Because of the lack of chemical resolution in the thermal decomposition window, trends in factors with oxidative aging remain difficult to interpret. Notably, the factors featuring *m/z* 44 (F1 in both Figure 11 and 13) increase with

photochemical aging, consistent with an increase in oxidized OA. In the wood BBOA, F2 (acetic acid) and F4 (less-oxidized organics) appear to peak at 3.4 days of equivalent aging, though the mechanisms driving this change remain uncertain. The PMF results obtained in this study will be used to develop appropriate standards for the TAG thermal decomposition window, allowing for more quantitative analysis and easier identification of mass spectral fragments in future field and laboratory work.

3.3 *m/z* 60 as a Tracer for both Primary and Aged BBOA

The signal eluting between minutes 27 and 32 of GC analysis results from the co-elution of multiple compounds, including levoglucosan. Like levoglucosan, most of these co-eluting species exhibit *m/z* 60 (dominated by the $C_2H_4O^+$ ion) as a major fragment in their mass spectra. These compounds are poorly resolved because the non-polar GC column is not designed to resolve such polar compounds. SICs at different levels of oxidation reveal that each compound within this retention time window reacts at a unique rate, allowing for the identification of different co-eluting species.

Wood and leaf BBOA *m/z* 60 single ion chromatograms (SICs) at each level of oxidation are given in Figure 15, and relative abundances of key *m/z* 60 fragmenting species in the TAG compound window are provided in Supplemental Information (Table S8). In the unaged oak wood BBOA chromatograms, approximately 82% of the TAG compound window *m/z* 60 signal has been identified as levoglucosan (retention time determined from authentic standards; Figure S13 in Supplemental Information), though other sugars and anhydro-sugars exist in lower abundances. While some levoglucosan (between 8.35% and 3.20%) is present in the oak leaf BBOA chromatograms, up to 60% of the TAG compound *m/z* 60 signal comes from quinic acid, which elutes beginning at minute 29 (retention time determined from authentic standards; Figure S13 in Supplemental Information). The differences in sources of *m/z* 60 between types of biomass illustrate that the *m/z* 60 signal in any given BBOA sample may be highly complex and dependent on the type of biomass burned.

In the leaf and wood BBOA, an increase in the *m/z* 60 signal was observed in the decomposition window from 0 to 9.8 days of equivalent aging. Deconvolution PMF results demonstrate that the *m/z* 60 decomposition signal co-elutes with *m/z* 43 and *m/z* 45 signals, which likely correspond to $C_2H_3O^+$ and CHO_2^+, respectively, and is unique from the mass spectrum of levoglucosan (Figure S14 in Supplemental Information). The co-elution of these three fragments and their relative integrated abundances provides evidence that organic acids constitute a portion of the decomposing OA. Further, the increase in the *m/z* 60 integrated signal suggests that these acids are formed during oxidative reactions occurring in the PAM chamber, either through heterogeneous oxidation of primary BBOA or condensation of oxidized SOA material.

Relative rates of decay for integrated *m/z* 60 fragmenting species are given in Figure 16. For leaf BBOA (Figure 16a), these compounds include levoglucosan, quinic acid, mannose, and octadecanoic acid, and for wood BBOA (Figure 16b), these include levoglucosan, guanosine, galactoheptulose, n-acetyl-d-galactosamine, and 1,6-anhydro-α-d-galactofuranose. The TAG decomposition window *m/z* 60 signal, total TAG compound window *m/z* 60 signal, and AMS f_{60} (the ratio of *m/z* 60 to the total signal; Ng et al., 2011) are also included in Figure 16a and 16b for comparison. All values have been normalized to the signal obtained at 0 days of equivalent aging. The normalized abundances for

TAG species were obtained by integrating each compound's *m/z* 60 signal at each level of oxidation, then dividing each peak area by the peak area obtained in the unaged chromatograms ("0 days"). As with TAG species, AMS f_{60} has been normalized at each level of oxidation to the AMS f_{60} obtained without photochemical aging.

Primary TAG species generally decrease in abundance with photochemical aging, though rates of decay vary depending on the compound. By contrast, in both wood and leaf BBOA, the TAG decomposition *m/z* 60 summed signal increases overall from zero to 9.8 days of equivalent aging, peaking at 3.4 days of aging. In the leaf BBOA, the AMS *m/z* 60 signal decreases by approximately 10% at 9.8 days of aging, while the AMS f_{60} in the wood BBOA is reduced to 50% of its original value at the highest level of oxidation. These trends in AMS f_{60} may reflect the combined effects of the oxidative decay of BBOA compounds, including sugars and anhydrosugars, and the formation of organic acids with functionalization reactions in the PAM chamber. Previous BBOA chemical characterization studies have identified organic acids as BBOA tracers (Falkovich et al., 2005; Lin et al., 2016; Mazzoleni et al., 2007), and Ortega, et al. report that organic acids formed through OFR-driven oxidation may contribute to net AMS *m/z* 60 (Ortega et al., 2013).

The OH·-driven oxidation kinetics of levoglucosan in BBOA have been investigated in previous chamber oxidation studies. For example, Kessler, et al. obtained a second order rate constant of $k_{LG} = (3.09 \pm 0.18) \times 10^{-13}$ cm^3 molec^{-1} s^{-1} from AMS measurements of OFR-oxidized levoglucosan particles (Kessler et al., 2010), while Hennigan, et al. obtained a rate constant of $k_{LG} = (1.1 \pm 0.5) \times 10^{-11}$ cm^3 molec^{-1} s^{-1} from smog chamber experiments (Hennigan et al., 2010). Lai, et al. obtained expressions for k_{LG} as a function of relative humidity and temperature in their own smog chamber experiments; at 25ºC and 30% relative humidity, $k_{LG} = 1.107 \times 10^{-11}$ cm^3 molec^{-1} s^{-1}, a value in good agreement with Hennigan, et al.'s results (Lai et al., 2014). Lai, et al. attribute the discrepancy between Kessler, et al.'s and Hennigan, et al.'s calculated k_{LG} to differences in both the levoglucosan detection method and experimental OH· concentration ranges. First, while Hennigan, et al. used offline filter collections to determine levoglucosan concentrations, Kessler, et al. took online measurements using an AMS and used *m/z* 144 as the marker fragment for levoglucosan. Lai, et al. explain that because the parent ion of *m/z* 162 was not used as the marker fragment in Kessler, et al.'s AMS measurements, any potential effects from reaction products cannot be fully isolated, possibly leading to an underestimate of levoglucosan decay. Additionally, Lai, et al. suggest that their own results may differ from those obtained by Kessler, et al. because they operated at much lower OH· concentrations. During our oxidation experiments, OH· concentrations ([OH·]) ranged from $10^9 - 10^{10}$ molec cm^{-3}, closer to the operating conditions of Kessler, et al. ([OH·] = $10^9 - 2 \times 10^{11}$ molec cm^{-3}; Kessler et al., 2010) than Lai, et al. ([OH·] = 3.50×10^7 molec cm^{-3}; Lai et al., 2014).

Figure 16c displays experimental relative abundances as functions of equivalent aging time for various TAG and AMS markers observed during wood BBOA oxidation, along with levoglucosan decay rates calculated using k_{LG} values obtained in previous studies (Kessler et al., 2010; Lai et al., 2014). In addition, AMS f_{60} values obtained for PAM-aged turkey oak BBOA (*Q. laevis*) during the FLAME-3 campaign (Ortega et al., 2013) are overlaid for comparison; the values plotted correspond to $f_{60} = 0.028$ at $OH_{exp} = 0$ molec cm^{-3} s and $f_{60} = 0.016$ at $OH_{exp} = 5.6 \times 10^{11}$ molec cm^{-3} s (approximately 4.3 days of equivalent aging based on their PAM reactor calibration), with each point normalized

to f_{60} = 0.028 (Ortega et al., 2013). While levoglucosan decays rapidly in the leaf BBOA with increasing OH_{exp}, levoglucosan in the wood BBOA is depleted more slowly. Levoglucosan is classified as semivolatile (at 25°C, $p_L°$ ~ 1.81×10^{-7} torr; ACD/Labs, 2017) and is therefore expected to partition between the gas and particle phases. The discrepancy in levoglucosan decay rates between wood and leaf BBOA could therefore be attributed to increased levoglucosan gas-to-particle phase partitioning in the wood BBOA, since levoglucosan concentrations are expected to be higher in oak wood BBOA than in oak leaf BBOA due to a higher typical presence of cellulose in oak wood (Jin et al., 2013; Suberkropp et al., 1976). OH· suppression, which could result from increased reactivity of OH· with other species at the particle surface, may also contribute to a slower rate of levoglucosan decay in wood BBOA than leaf BBOA. The AMS *m/z* 60 signal agrees well with the levoglucosan decay rate calculated using Kessler, et al.'s k_{LG}, and decreases with increasing OH_{exp}, though displays less overall decay compared to levoglucosan measured by TAG. Our results demonstrate that although *m/z* 60 may be an effective tracer for levoglucosan and primary BBOA under certain conditions, the formation of organic acids through photochemical aging may also impact AMS *m/z* 60 and should be considered when using the AMS to track levoglucosan and primary BBOA in future studies. Furthermore, these results illustrate the utility of TAG data in interpreting AMS bulk OA measurements, as it gives both molecular characterization as well as additional insight on the chemical makeup of the most aged OA through evaluation of thermal decomposition components.

4 Conclusions and Atmospheric Implications

The experimental methods presented in this work allow repeatable collection, oxidation, and molecular-level analysis of source-specific BBOA. The identification of molecular tracers unique to leaf and wood fuels can aid apportionment of BBOA to different plant fractions. For example, based on our results, a BBOA plume exhibiting high concentrations of aliphatic leaf wax components may be attributed to canopy or leaf litter devolatilization and combustion, while a plume with high concentrations of levoglucosan and lignin decomposition products could be attributed to heartwood combustion. Additionally, our results suggest that certain molecular tracers of interest may persist after 3 days of equivalent aging and may even increase in abundance with atmospheric aging due to reaction or gas-to-particle partitioning. The relative rates of OH·-driven decay obtained from TAG measurements may thus inform future field observations where molecular speciation information is obtained for photochemically aged plumes.

Although the TAG's OA analysis capability has historically been limited by poor mass throughput of highly oxygenated species, we demonstrate here that the TAG decomposition window can be used to gain a better understanding of the molecular composition of oxidized BBOA. While the decomposition window does not provide chemical composition information with molecular resolution, the chromatogram binning PMF results allow identification of different co-eluting factors, many of which correspond to molecular fragments that could be used as source-specific BBOA tracers in future field studies.

For both types of BBOA, the *m/z* 44 signal in the TAG decomposition window increases with photochemical aging, confirming that this signal indicates the presence of thermally labile oxygenated OA and may provide information on the photochemical age of the aerosol sample. However, our observations suggest that the utility of decomposition *m/z* 44 as a quantifiable tracer for aged OA varies depending on OA type. For oak wood BBOA, the TAG decomposition

m/z 44 signal correlates well with AMS $\overline{OS_C}$, suggesting that for this type of BBOA, the decomposition *m/z* 44 abundance could be used to estimate the aerosol's oxidation state. By contrast, the correlation between TAG decomposition *m/z* 44 and AMS $\overline{OS_C}$ is not significant for PAM-aged oak leaf BBOA, perhaps because compounds formed with photochemical aging of leaf BBOA are less thermally labile and more resistant to thermal decomposition than those found in aged wood BBOA.

From the TAG data, we observe two competing effects driving the overall *m/z* 60 signal measured in the AMS; while many primary BBOA components exhibiting a characteristic *m/z* 60 fragment, including anhydrosugars like levoglucosan, were depleted with photochemical aging, an enhanced *m/z* 60 signal in the decomposition window may signal increased formation of organic acids in the PAM reactor. Both processes have been reported in previous literature, though the oxidative depletion of primary BBOA is most typically thought to drive AMS *m/z* 60 trends in field and laboratory studies. Our data suggest that although AMS measurements provide useful chemical composition information on bulk OA, laboratory studies with molecular-level measurements are needed to complement AMS data and provide a more complete understanding of processes occurring in the atmosphere.

The mechanisms driving compositional changes in BBOA remain difficult to interpret. While many compounds observed in this study are clearly depleted through functionalization reactions, some species may be subjected to phase partitioning effects in addition to PAM-driven oxidation. In particular, the enhancement in TAG thermal decomposition *m/z* 44 and *m/z* 60 may occur due to formation of SOA through oxidation and condensation of low-volatility gases, heterogeneous functionalization of compounds in the particle phase, or a combination of these processes. Future studies will focus on investigating the role of phase partitioning in OA chemical composition within BBOA plumes, with emphasis on the thermally labile material eluting in the TAG thermal decomposition window. In addition, different types of biomass will be tested to explore the dependence of phase partitioning and photochemical aging effects on fuel type, broadening the applicability of these techniques to future field measurements.

Acknowledgements

The material presented is based on work supported by the National Science Foundation (award no. 1437933). The authors would also like to acknowledge support from the International Center for Energy, Environment and Sustainability (INCEES) and the McDonnell Academy Global Energy and Environment Partnership (MAGEEP) at Washington University in St. Louis.

References

ACD/Labs: Advanced Chemistry Development (ACD/Labs) Software V11.02 (© 1994–2012 ACD/Labs), Retrieved from http://www.cas.org/products/scifinder, 11 May, 2017.

Appel, B. R., Tokiwa, Y., Hsu, J., Kothny, E. L. and Hahn, E.: Visibility as related to atmospheric aerosol constituents, Atmospheric Environ. 1967, 19(9), 1525–1534, doi:10.1016/0004-6981(85)90290-2, 1985.

Bond, T. C., Streets, D. G., Yarber, K. F., Nelson, S. M., Woo, J.-H. and Klimont, Z.: A technology-based global inventory of black and organic carbon emissions from combustion, J. Geophys. Res. Atmospheres, 109(D14), D14203, doi:10.1029/2003JD003697, 2004.

Canagaratna, M. R., Jayne, J. T., Jimenez, J. L., Allan, J. D., Alfarra, M. R., Zhang, Q., Onasch, T. B., Drewnick, F., Coe, H., Middlebrook, A., Delia, A., Williams, L. R., Trimborn, A. M., Northway, M. J., DeCarlo, P. F., Kolb, C. E., Davidovits, P. and Worsnop, D. R.: Chemical and microphysical characterization of ambient aerosols with the aerodyne aerosol mass spectrometer, Mass Spectrom. Rev., 26(2), 185–222, doi:10.1002/mas.20115, 2007.

Capes, G., Johnson, B., McFiggans, G., Williams, P. I., Haywood, J. and Coe, H.: Aging of biomass burning aerosols over West Africa: Aircraft measurements of chemical composition, microphysical properties, and emission ratios, J. Geophys. Res. Atmospheres, 113(D23), D00C15, doi:10.1029/2008JD009845, 2008.

Cubison, M. J., Ortega, A. M., Hayes, P. L., Farmer, D. K., Day, D., Lechner, M. J., Brune, W. H., Apel, E., Diskin, G. S., Fisher, J. A., Fuelberg, H. E., Hecobian, A., Knapp, D. J., Mikoviny, T., Riemer, D., Sachse, G. W., Sessions, W., Weber, R. J., Weinheimer, A. J., Wisthaler, A. and Jimenez, J. L.: Effects of aging on organic aerosol from open biomass burning smoke in aircraft and laboratory studies, Atmos Chem Phys, 11(23), 12049–12064, doi:10.5194/acp-11-12049-2011, 2011.

D'Anna, B., Andresen, Ø., Gefen, Z. and Nielsen, C. J.: Kinetic study of OH and NO3 radical reactions with 14 aliphatic aldehydes, Phys. Chem. Chem. Phys., 3(15), 3057–3063, doi:10.1039/B103623H, 2001.

DeCarlo, P. F., Kimmel, J. R., Trimborn, A., Northway, M. J., Jayne, J. T., Aiken, A. C., Gonin, M., Fuhrer, K., Horvath, T., Docherty, K. S., Worsnop, D. R. and Jimenez, J. L.: Field-Deployable, High-Resolution, Time-of-Flight Aerosol Mass Spectrometer, Anal. Chem., 78(24), 8281–8289, doi:10.1021/ac061249n, 2006.

Falkovich, A. H., Graber, E. R., Schkolnik, G., Rudich, Y., Maenhaut, W. and Artaxo, P.: Low molecular weight organic acids in aerosol particles from Rondônia, Brazil, during the biomass-burning, transition and wet periods, Atmos Chem Phys, 5(3), 781–797, doi:10.5194/acp-5-781-2005, 2005.

Fine, P. M., Cass, G. R. and Simoneit, B. R. T.: Organic compounds in biomass smoke from residential wood combustion: Emissions characterization at a continental scale, J. Geophys. Res. Atmospheres, 107(D21), Art. No 8349, 2002.

Forman, G. S., Hauser, A. B. and Adda, S. M.: Life cycle analysis of gas to liquids (GTL) derived linear alkyl benzene, J. Clean. Prod., 80, 30–37, doi:10.1016/j.jclepro.2014.05.058, 2014.

Fraser, M. P. and Lakshmanan, K.: Using Levoglucosan as a Molecular Marker for the Long-Range Transport of Biomass Combustion Aerosols, Environ. Sci. Technol., 34(21), 4560–4564, doi:10.1021/es991229l, 2000.

Goldstein, A. H. and Galbally, I. E.: Known and Unexplored Organic Constituents in the Earth's Atmosphere, Environ. Sci. Technol., 41(5), 1514–1521, doi:10.1021/es072476p, 2007.

Grieshop, A. P., Logue, J. M., Donahue, N. M. and Robinson, A. L.: Laboratory investigation of photochemical oxidation of organic aerosol from wood fires 1: measurement and simulation of organic aerosol evolution, Atmos Chem Phys, 9(4), 1263–1277, doi:10.5194/acp-9-1263-2009, 2009.

Gulz, P. G. and Boor, G.: Seasonal Variations in Epicuticular Wax Ultrastructures of *Quercus robur* Leaves, Z Naturforsch, 47c, 807–814, 1992.

Hennigan, C. J., Sullivan, A. P., Collett, J. L. and Robinson, A. L.: Levoglucosan stability in biomass burning particles exposed to hydroxyl radicals, Geophys. Res. Lett., 37(9), doi:10.1029/2010GL043088, 2010.

Hoffmann, D., Tilgner, A., Iinuma, Y. and Herrmann, H.: Atmospheric stability of levoglucosan: a detailed laboratory and modeling study, Environ. Sci. Technol., 44(2), 694–699, doi:10.1021/es902476f, 2010.

Jin, W., Singh, K. and Zondlo, J.: Pyrolysis Kinetics of Physical Components of Wood and Wood-Polymers Using Isoconversion Method, Agriculture, 3(1), 12–32, doi:10.3390/agriculture3010012, 2013.

Kampa, M. and Castanas, E.: Human health effects of air pollution, Environ. Pollut., 151(2), 362–367, doi:10.1016/j.envpol.2007.06.012, 2008.

Kanakidou, M., Seinfeld, J. H., Pandis, S. N., Barnes, I., Dentener, F. J., Facchini, M. C., Van Dingenen, R., Ervens, B., Nenes, A., Nielsen, C. J., Swietlicki, E., Putaud, J. P., Balkanski, Y., Fuzzi, S., Horth, J., Moortgat, G. K., Winterhalter, R., Myhre, C. E. L., Tsigaridis, K., Vignati, E., Stephanou, E. G. and Wilson, J.: Organic aerosol and global climate modelling: a review, Atmos Chem Phys, 5(4), 1053–1123, doi:10.5194/acp-5-1053-2005, 2005.

Kang, E., Root, M. J., Toohey, D. W. and Brune, W. H.: Introducing the concept of Potential Aerosol Mass (PAM), Atmos Chem Phys, 7(22), 5727–5744, doi:10.5194/acp-7-5727-2007, 2007.

Kessler, S. H., Smith, J. D., Che, D. L., Worsnop, D. R., Wilson, K. R. and Kroll, J. H.: Chemical Sinks of Organic Aerosol: Kinetics and Products of the Heterogeneous Oxidation of Erythritol and Levoglucosan, Environ. Sci. Technol., 44(18), 7005–7010, doi:10.1021/es101465m, 2010.

Kreisberg, N. M., Hering, S. V., Williams, B. J., Worton, D. R. and Goldstein, A. H.: Quantification of Hourly Speciated Organic Compounds in Atmospheric Aerosols, Measured by an In-Situ Thermal Desorption Aerosol Gas Chromatograph (TAG), Aerosol Sci. Technol., 43(1), 38–52, doi:10.1080/02786820802459583, 2009.

Kroll, J. H., Smith, J. D., Che, D. L., Kessler, S. H., Worsnop, D. R. and Wilson, K. R.: Measurement of fragmentation and functionalization pathways in the heterogeneous oxidation of oxidized organic aerosol, Phys. Chem. Chem. Phys., 11(36), 8005–8014, doi:10.1039/B905289E, 2009.

Kroll, J. H., Donahue, N. M., Jimenez, J. L., Kessler, S. H., Canagaratna, M. R., Wilson, K. R., Altieri, K. E., Mazzoleni, L. R., Wozniak, A. S., Bluhm, H., Mysak, E. R., Smith, J. D., Kolb, C. E. and Worsnop, D. R.: Carbon oxidation state as a metric for describing the chemistry of atmospheric organic aerosol, Nat. Chem., 3(2), 133–139, doi:10.1038/nchem.948, 2011.

Lai, C., Liu, Y., Ma, J., Ma, Q. and He, H.: Degradation kinetics of levoglucosan initiated by hydroxyl radical under different environmental conditions, Atmos. Environ., 91, 32–39, doi:10.1016/j.atmosenv.2014.03.054, 2014.

Lambe, A. T., Logue, J. M., Kreisberg, N. M., Hering, S. V., Worton, D. R., Goldstein, A. H., Donahue, N. M. and Robinson, A. L.: Apportioning black carbon to sources using highly time-resolved ambient measurements of organic molecular markers in Pittsburgh, Atmos. Environ., 43(25), 3941–3950, doi:10.1016/j.atmosenv.2009.04.057, 2009.

Lambe, A. T., Ahern, A. T., Williams, L. R., Slowik, J. G., Wong, J. P. S., Abbatt, J. P. D., Brune, W. H., Ng, N. L., Wright, J. P., Croasdale, D. R., Worsnop, D. R., Davidovits, P. and Onasch, T. B.: Characterization of aerosol photooxidation flow reactors: heterogeneous oxidation, secondary organic aerosol formation and cloud condensation nuclei activity measurements, Atmos Meas Tech, 4(3), 445–461, doi:10.5194/amt-4-445-2011, 2011.

Lee, T., Sullivan, A. P., Mack, L., Jimenez, J. L., Kreidenweis, S. M., Onasch, T. B., Worsnop, D. R., Malm, W., Wold, C. E., Hao, W. M. and Jr, J. L. C.: Chemical Smoke Marker Emissions During Flaming and Smoldering Phases of Laboratory Open Burning of Wildland Fuels, Aerosol Sci. Technol., 44(9), i–v, doi:10.1080/02786826.2010.499884, 2010.

Li, R., Palm, B. B., Ortega, A. M., Hlywiak, J., Hu, W., Peng, Z., Day, D. A., Knote, C., Brune, W. H., de Gouw, J. A. and Jimenez, J. L.: Modeling the Radical Chemistry in an Oxidation Flow Reactor: Radical Formation and Recycling, Sensitivities, and the OH Exposure Estimation Equation, J. Phys. Chem. A, 119(19), 4418–4432, doi:10.1021/jp509534k, 2015.

Lin, P., Aiona, P. K., Li, Y., Shiraiwa, M., Laskin, J., Nizkorodov, S. A. and Laskin, A.: Molecular Characterization of Brown Carbon in Biomass Burning Aerosol Particles, Environ. Sci. Technol., 50(21), 11815–11824, doi:10.1021/acs.est.6b03024, 2016.

Locker, H. B.: The use of levoglucosan to assess the environmental impact of residential wood-burning on air quality, PhD Thesis, Dartmouth College, Hanover, NH, 137 pp., 1988.

Mao, J., Ren, X., Brune, W. H., Olson, J. R., Crawford, J. H., Fried, A., Huey, L. G., Cohen, R. C., Heikes, B., Singh, H. B., Blake, D. R., Sachse, G. W., Diskin, G. S., Hall, S. R. and Shetter, R. E.: Airborne measurement of OH reactivity during INTEX-B, Atmos Chem Phys, 9(1), 163–173, doi:10.5194/acp-9-163-2009, 2009.

May, A. A., Levin, E. J. T., Hennigan, C. J., Riipinen, I., Lee, T., Collett, J. L., Jimenez, J. L., Kreidenweis, S. M. and Robinson, A. L.: Gas-particle partitioning of primary organic aerosol emissions: 3. Biomass burning, J. Geophys. Res. Atmospheres, 118(19), 2013JD020286, doi:10.1002/jgrd.50828, 2013.

Mazzoleni, L. R., Zielinska, B. and Moosmüller, H.: Emissions of Levoglucosan, Methoxy Phenols, and Organic Acids from Prescribed Burns, Laboratory Combustion of Wildland Fuels, and Residential Wood Combustion, Environ. Sci. Technol., 41(7), 2115–2122, doi:10.1021/es061702c, 2007.

Ng, N. L., Canagaratna, M. R., Zhang, Q., Jimenez, J. L., Tian, J., Ulbrich, I. M., Kroll, J. H., Docherty, K. S., Chhabra, P. S., Bahreini, R., Murphy, S. M., Seinfeld, J. H., Hildebrandt, L., Donahue, N. M., DeCarlo, P. F., Lanz, V. A., Prévôt, A. S. H., Dinar, E., Rudich, Y. and Worsnop, D. R.: Organic aerosol components observed in Northern Hemispheric datasets from Aerosol Mass Spectrometry, Atmos Chem Phys, 10(10), 4625–4641, doi:10.5194/acp-10-4625-2010, 2010.

Ng, N. L., Canagaratna, M. R., Jimenez, J. L., Chhabra, P. S., Seinfeld, J. H. and Worsnop, D. R.: Changes in organic aerosol composition with aging inferred from aerosol mass spectra, Atmos Chem Phys, 11(13), 6465–6474, doi:10.5194/acp-11-6465-2011, 2011a.

Ng, N. L., Canagaratna, M. R., Jimenez, J. L., Zhang, Q., Ulbrich, I. M. and Worsnop, D. R.: Real-Time Methods for Estimating Organic Component Mass Concentrations from Aerosol Mass Spectrometer Data, Environ. Sci. Technol., 45(3), 910–916, doi:10.1021/es102951k, 2011b.

Niki, H., Maker, P. D., Savage, C. M. and Breitenbach, L. P.: Relative rate constants for the reaction of hydroxyl radical with aldehydes, J. Phys. Chem., 82(2), 132–134, doi:10.1021/j100491a002, 1978.

Oros, D. R. and Simoneit, B. R. T.: Identification of Molecular Tracers in Organic Aerosols from Temperate Climate Vegetation Subjected to Biomass Burning, Aerosol Sci. Technol., 31(6), 433–445, doi:10.1080/027868299303986, 1999.

Ortega, A. M., Day, D. A., Cubison, M. J., Brune, W. H., Bon, D., de Gouw, J. A. and Jimenez, J. L.: Secondary organic aerosol formation and primary organic aerosol oxidation from biomass-burning smoke in a flow reactor during FLAME-3, Atmos Chem Phys, 13(22), 11551–11571, doi:10.5194/acp-13-11551-2013, 2013.

Paatero, P.: Least squares formulation of robust non-negative factor analysis, Chemom. Intell. Lab. Syst., 37(1), 23–35, doi:10.1016/S0169-7439(96)00044-5, 1997.

Peng, Z., Day, D. A., Stark, H., Li, R., Lee-Taylor, J., Palm, B. B., Brune, W. H. and Jimenez, J. L.: HOx radical chemistry in oxidation flow reactors with low-pressure mercury lamps systematically examined by modeling, Atmos Meas Tech, 8(11), 4863–4890, doi:10.5194/amt-8-4863-2015, 2015.

Rogge, W. F., Hildemann, L. M., Mazurek, M. A. and Cass, G. R.: Sources of Fine Organic Aerosol. 9. Pine, Oak, and Synthetic Log Combustion in Residential Fireplaces, Environ. Sci. Technol., 32(1), 13–22, doi:10.1021/es960930b, 1998.

Simoneit, B. R. T., Schauer, J. J., Nolte, C. G., Oros, D. R., Elias, V. O., Fraser, M. P., Rogge, W. F. and Cass, G. R.: Levoglucosan, a tracer for cellulose in biomass burning and atmospheric particles, Atmos. Environ., 33(2), 173–182, doi:10.1016/S1352-2310(98)00145-9, 1999.

Simoneit, B. R. T., Rogge, W. F., Lang, Q. and Jaffé, R.: Molecular characterization of smoke from campfire burning of pine wood (Pinus elliottii), Chemosphere - Glob. Change Sci., 2(1), 107–122, doi:10.1016/S1465-9972(99)00048-3, 2000.

Simoneit, B. R. T., Kobayashi, M., Mochida, M., Kawamura, K. and Huebert, B. J.: Aerosol particles collected on aircraft flights over the northwestern Pacific region during the ACE-Asia campaign: Composition and major sources of the organic compounds, J. Geophys. Res. Atmospheres, 109(D19), D19S09, doi:10.1029/2004JD004565, 2004.

Stein, S. E. and Scott, D. R.: Optimization and testing of mass spectral library search algorithms for compound identification, J. Am. Soc. Mass Spectrom., 5(9), 859–866, doi:10.1016/1044-0305(94)87009-8, 1994.

Stockwell, C. E., Veres, P. R., Williams, J. and Yokelson, R. J.: Characterization of biomass burning emissions from cooking fires, peat, crop residue, and other fuels with high-resolution proton-transfer-reaction time-of-flight mass spectrometry, Atmos Chem Phys, 15(2), 845–865, doi:10.5194/acp-15-845-2015, 2015.

Suberkropp, K., Godshalk, G. L. and Klug, M. J.: Changes in the Chemical Composition of Leaves During Processing in a Woodland Stream, Ecology, 57(4), 720–727, doi:10.2307/1936185, 1976.

Ulbrich, I. M., Canagaratna, M. R., Zhang, Q., Worsnop, D. R. and Jimenez, J. L.: Interpretation of organic components from Positive Matrix Factorization of aerosol mass spectrometric data, Atmos Chem Phys, 9(9), 2891–2918, doi:10.5194/acp-9-2891-2009, 2009.

Watson, J. T. and Sparkman, O. D.: Introduction to Mass Spectrometry: Instrumentation, Applications, and Strategies for Data Interpretation, 4th ed., John Wiley & Sons Ltd, West Sussex, England., 2007.

Williams, B. J., Goldstein, A. H., Kreisberg, N. M. and Hering, S. V.: An In-Situ Instrument for Speciated Organic Composition of Atmospheric Aerosols: Thermal Desorption Aerosol GC/MS-FID (TAG), Aerosol Sci. Technol., 40(8), 627–638, doi:10.1080/02786820600754631, 2006.

Williams, B. J., Goldstein, A. H., Millet, D. B., Holzinger, R., Kreisberg, N. M., Hering, S. V., White, A. B., Worsnop, D. R., Allan, J. D. and Jimenez, J. L.: Chemical speciation of organic aerosol during the International Consortium for Atmospheric Research on Transport and Transformation 2004: Results from in situ measurements, J. Geophys. Res. Atmospheres, 112(D10), D10S26, doi:10.1029/2006JD007601, 2007.

Williams, B. J., Goldstein, A. H., Kreisberg, N. M., Hering, S. V., Worsnop, D. R., Ulbrich, I. M., Docherty, K. S. and Jimenez, J. L.: Major components of atmospheric organic aerosol in southern California as determined by hourly measurements of source marker compounds, Atmos Chem Phys, 10(23), 11577–11603, doi:10.5194/acp-10-11577-2010, 2010.

Williams, B. J., Jayne, J. T., Lambe, A. T., Hohaus, T., Kimmel, J. R., Sueper, D., Brooks, W., Williams, L. R., Trimborn, A. M., Martinez, R. E., Hayes, P. L., Jimenez, J. L., Kreisberg, N. M., Hering, S. V., Worton, D. R., Goldstein, A. H. and Worsnop, D. R.: The First Combined Thermal Desorption Aerosol Gas Chromatograph—Aerosol Mass Spectrometer (TAG-AMS), Aerosol Sci. Technol., 48(4), 358–370, doi:10.1080/02786826.2013.875114, 2014.

Williams, B. J., Zhang, Y., Zuo, X., Martinez, R. E., Walker, M. J., Kreisberg, N. M., Goldstein, A. H., Docherty, K. S. and Jimenez, J. L.: Organic and inorganic decomposition products from the thermal desorption of atmospheric particles, Atmos Meas Tech, 9(4), 1569–1586, doi:10.5194/amt-9-1569-2016, 2016.

Wong, Z., Chen, K. and Li, J.: Formation of Vanillin and Syringaldehyde in an Oxygen Delignification Process, BioResources, 5(3), 1509–1516, doi:10.15376/biores.5.3.1509-1516, 2010.

Worton, D. R., Goldstein, A. H., Farmer, D. K., Docherty, K. S., Jimenez, J. L., Gilman, J. B., Kuster, W. C., de Gouw, J., Williams, B. J., Kreisberg, N. M., Hering, S. V., Bench, G., McKay, M., Kristensen, K., Glasius, M.,

790 Surratt, J. D. and Seinfeld, J. H.: Origins and composition of fine atmospheric carbonaceous aerosol in the Sierra Nevada Mountains, California, Atmos Chem Phys, 11(19), 10219–10241, doi:10.5194/acp-11-10219-2011, 2011.

Zhang, Q., Jimenez, J. L., Canagaratna, M. R., Allan, J. D., Coe, H., Ulbrich, I., Alfarra, M. R., Takami, A., Middlebrook, A. M., Sun, Y. L., Dzepina, K., Dunlea, E., Docherty, K., DeCarlo, P. F., Salcedo, D., Onasch, T., Jayne, J. T., Miyoshi, T., Shimono, A., Hatakeyama, S., Takegawa, N., Kondo, Y., Schneider, J., Drewnick, F., 795 Borrmann, S., Weimer, S., Demerjian, K., Williams, P., Bower, K., Bahreini, R., Cottrell, L., Griffin, R. J., Rautiainen, J., Sun, J. Y., Zhang, Y. M. and Worsnop, D. R.: Ubiquity and dominance of oxygenated species in organic aerosols in anthropogenically-influenced Northern Hemisphere midlatitudes, Geophys. Res. Lett., 34(13), L13801, doi:10.1029/2007GL029979, 2007.

Zhang, Y., Williams, B. J., Goldstein, A. H., Docherty, K., Ulbrich, I. M. and Jimenez, J. L.: A Technique for Rapid 800 Gas Chromatography Analysis Applied to Ambient Organic Aerosol Measurements from the Thermal Desorption Aerosol Gas Chromatograph (TAG), Aerosol Sci. Technol., 48(11), 1166–1182, doi:10.1080/02786826.2014.967832, 2014.

Zhang, Y., Williams, B. J., Goldstein, A. H., Docherty, K. S. and Jimenez, J. L.: A technique for rapid source apportionment applied to ambient organic aerosol measurements from a thermal desorption aerosol gas 805 chromatograph (TAG), Atmos Meas Tech, 9(11), 5637–5653, doi:10.5194/amt-9-5637-2016, 2016.

810

815

Atmos. Chem. Phys. Discuss., https://doi.org/10.5194/acp-2017-576
Manuscript under review for journal Atmos. Chem. Phys.
Discussion started: 5 July 2017

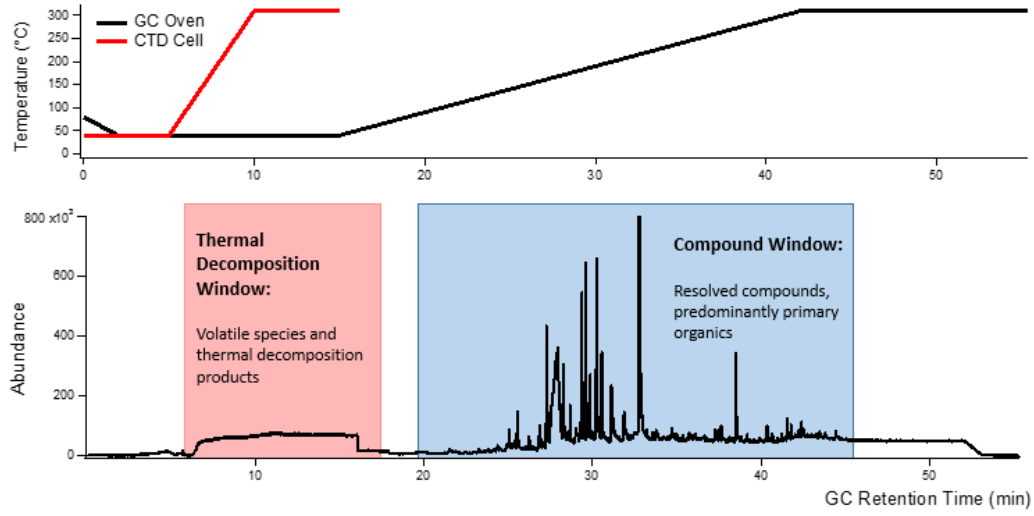

820 **Figure 1:** An example TAG chromatogram with GC oven and TAG collection and thermal desorption (CTD) cell temperature ramp programs.

Atmos. Chem. Phys. Discuss., https://doi.org/10.5194/acp-2017-576
Manuscript under review for journal Atmos. Chem. Phys.
Discussion started: 5 July 2017

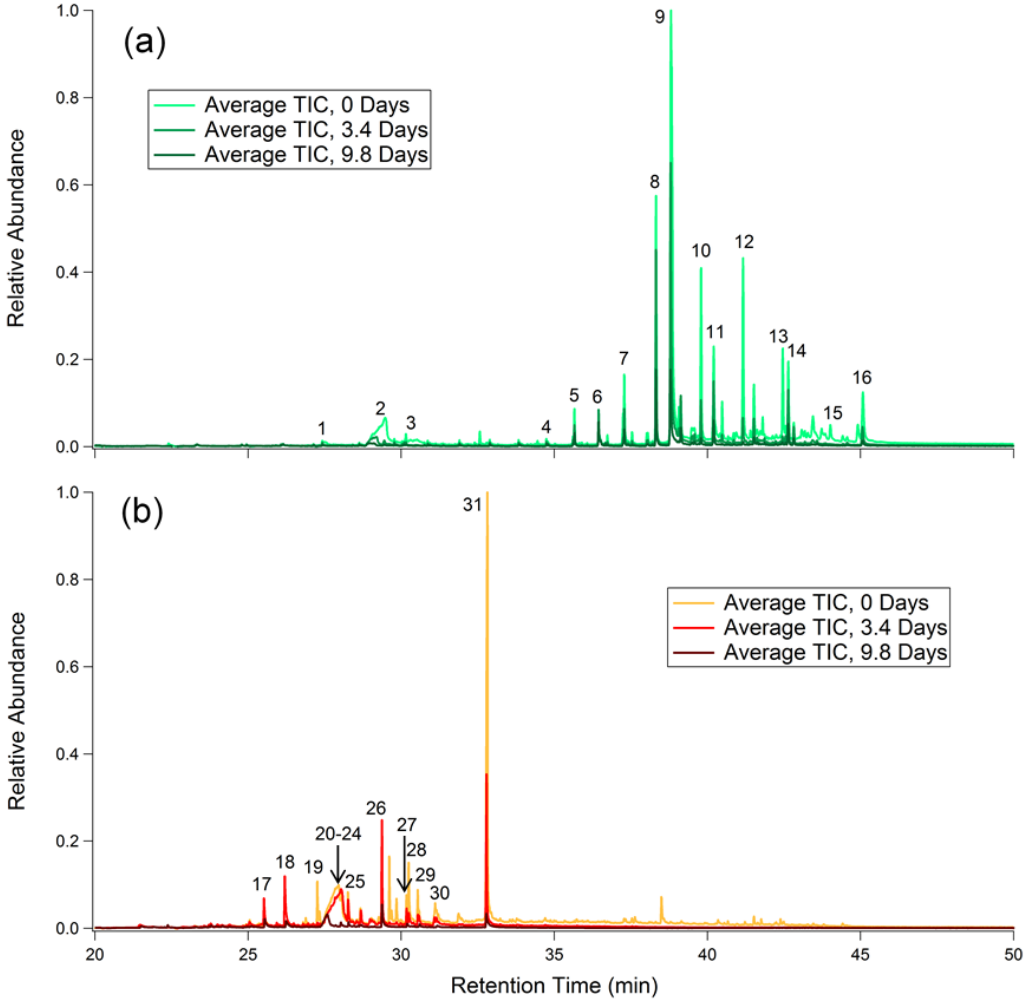

825 **Figure 2.** Chromatograms for **(a)** leaf BBOA and **(b)** heartwood BBOA at different levels of oxidation. Corresponding names and structures for numbered compounds are given in Tables S3-S4 and Figures S5-S6. For each plot, all traces are normalized to the point of highest abundance within the average unaged chromatogram.

830

Atmos. Chem. Phys. Discuss., https://doi.org/10.5194/acp-2017-576
Manuscript under review for journal Atmos. Chem. Phys.
Discussion started: 5 July 2017

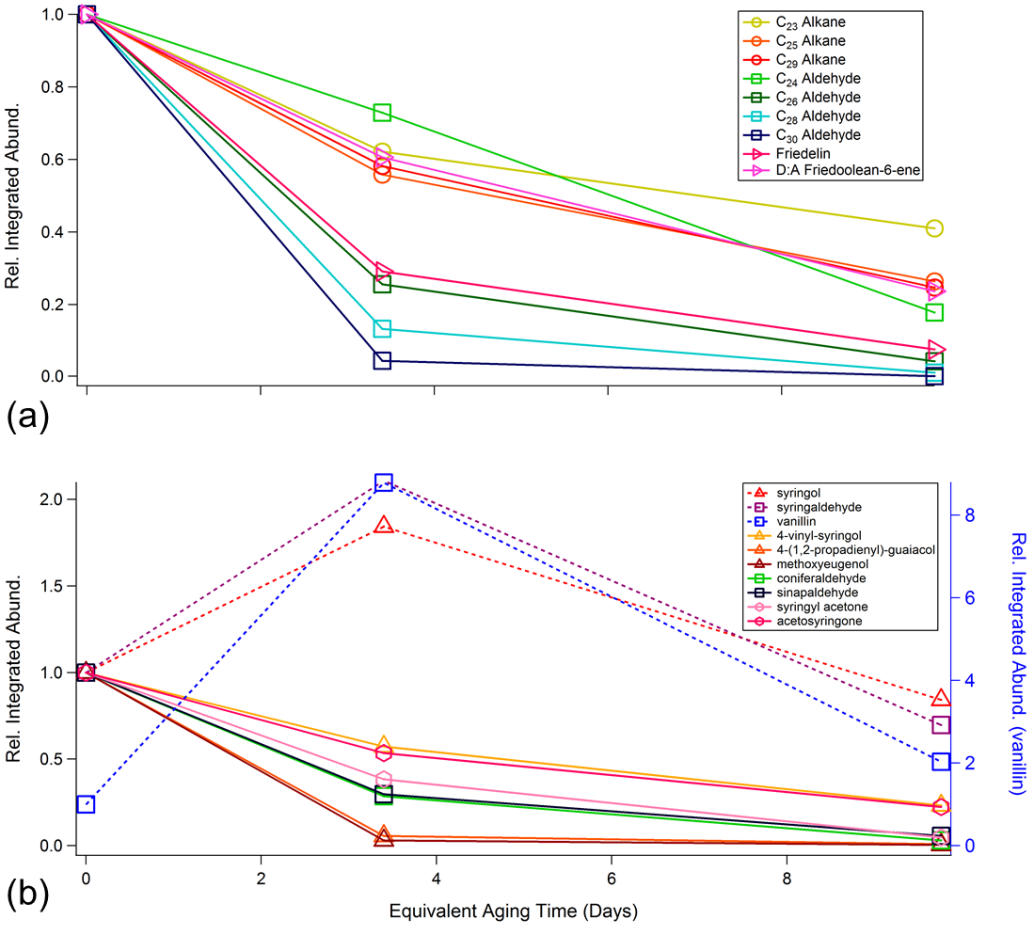

Figure 3: Relative changes in integrated abundance as a function of equivalent aging time for primary compounds identified in **(a)** oak leaf BBOA chromatograms, and **(b)** oak wood BBOA chromatograms. For each compound, the integrated abundances were first normalized to appropriate volume concentrations, then subsequently normalized to corresponding abundances at no oxidation ("0 days").

Atmos. Chem. Phys. Discuss., https://doi.org/10.5194/acp-2017-576
Manuscript under review for journal Atmos. Chem. Phys.
Discussion started: 5 July 2017

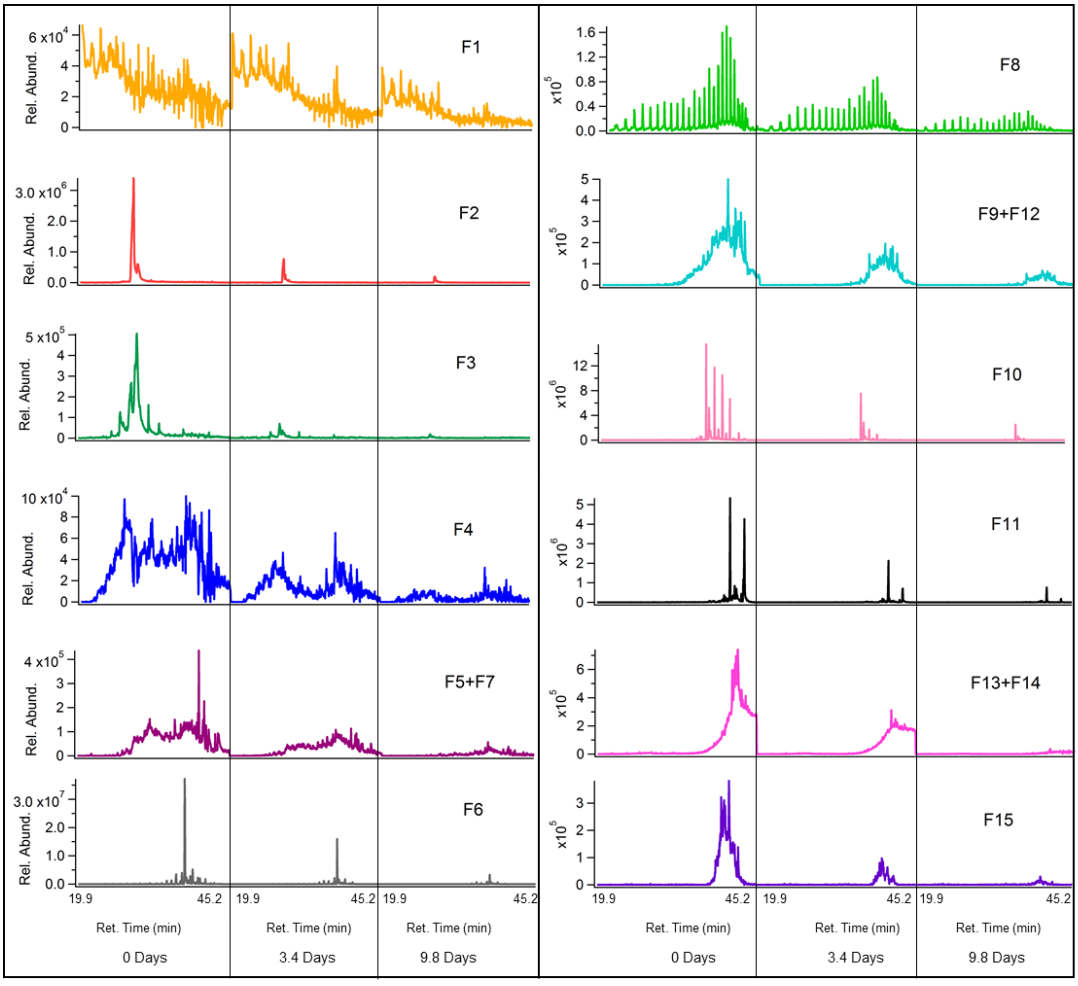

Figure 4: Average binned chromatograms for factors 1-15 (F1-15) in PMF 15-factor solution on TAG oak leaf BBOA compound window data. Relevant plots obtained in PMF calculations are provided in Supplemental Information (Figures 9a and 10a). These chromatograms were obtained from PMF calculations by averaging binned data corresponding to triplicate chromatograms at each level of oxidation. The triplicate-averaged binned chromatograms at each equivalent aging time are displayed in one trace; different aging times are demarcated with vertical lines across the x-axis.

Atmos. Chem. Phys. Discuss., https://doi.org/10.5194/acp-2017-576
Manuscript under review for journal Atmos. Chem. Phys.
Discussion started: 5 July 2017

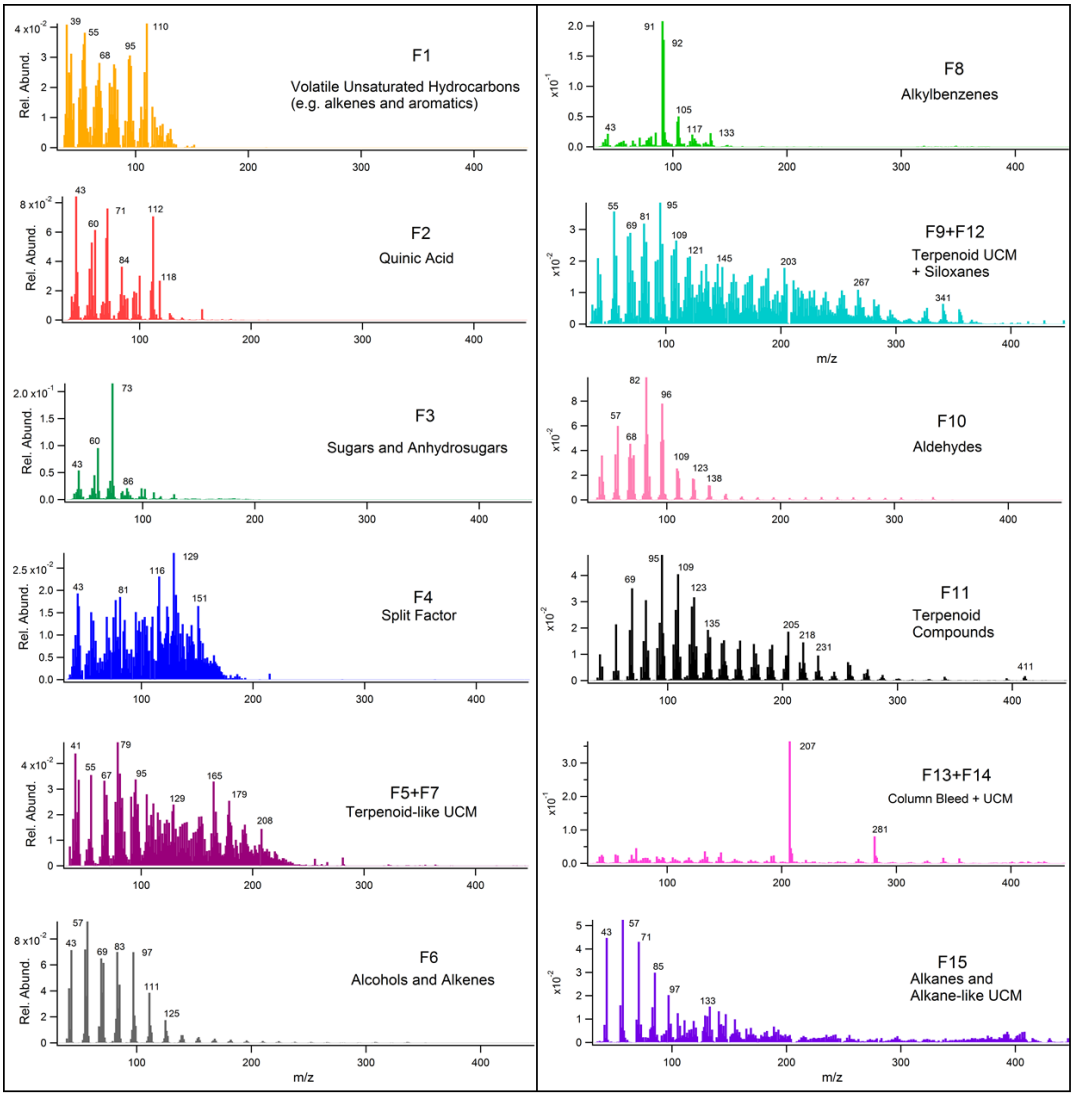

Figure 5: Mass spectra for factors 1-15 (F1-15) in PMF 15-factor solution on TAG oak leaf BBOA compound window data. Relevant plots obtained in PMF calculations are provided in Supplemental Information (Figures 9a and 10a).

Atmos. Chem. Phys. Discuss., https://doi.org/10.5194/acp-2017-576
Manuscript under review for journal Atmos. Chem. Phys.
Discussion started: 5 July 2017

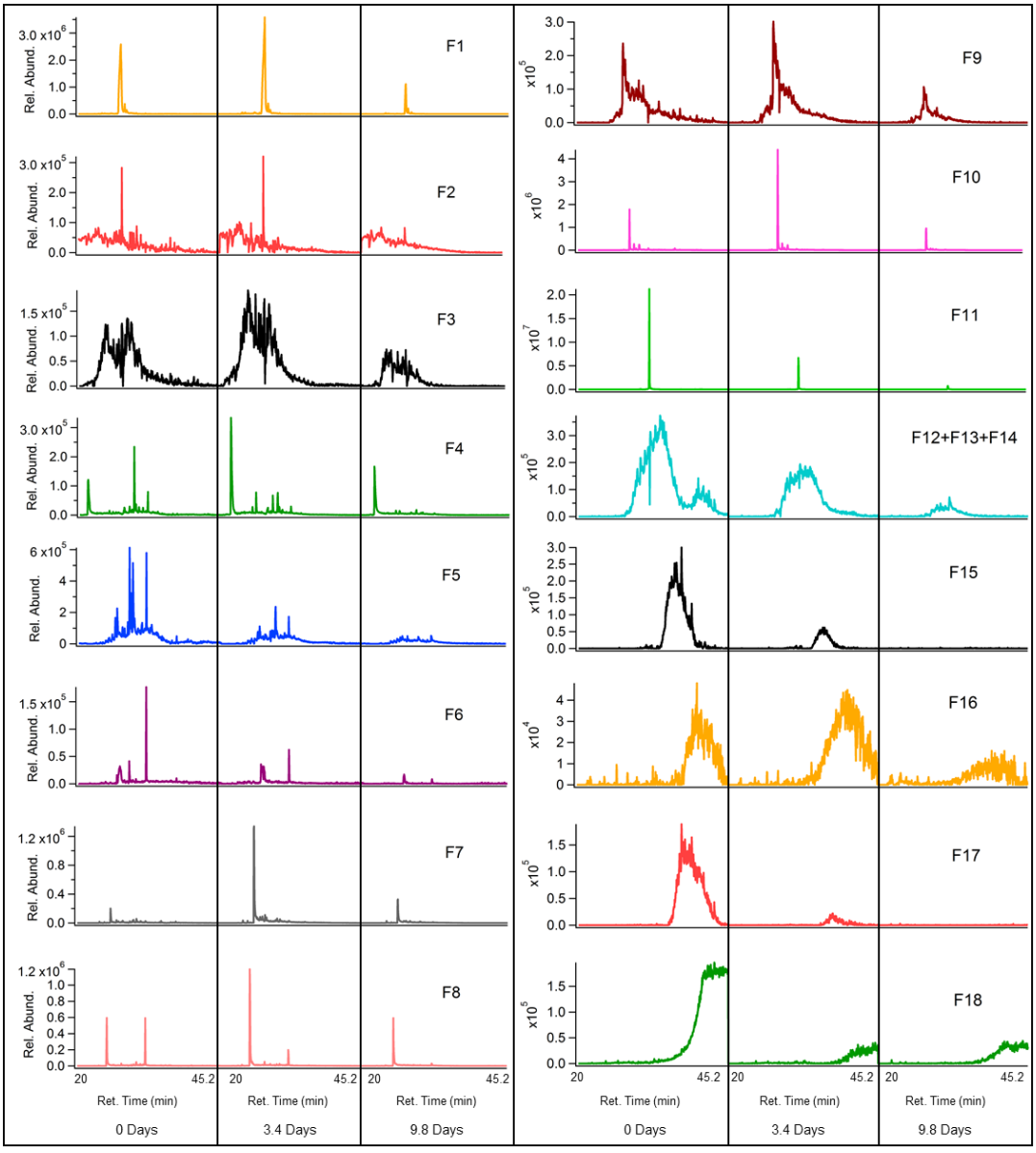

Figure 6: Average binned chromatograms for factors 1-18 (F1-18) in PMF 18-factor solution on TAG oak wood BBOA compound window data. Relevant plots obtained in PMF calculations are provided in Supplemental Information (Figures 9b and 10b). These chromatograms were obtained from PMF calculations by averaging binned data corresponding to triplicate chromatograms at each level of oxidation. The triplicate-averaged binned chromatograms at each equivalent aging time are displayed in one trace; different aging times are demarcated with vertical lines across the x-axis.

Atmos. Chem. Phys. Discuss., https://doi.org/10.5194/acp-2017-576
Manuscript under review for journal Atmos. Chem. Phys.
Discussion started: 5 July 2017

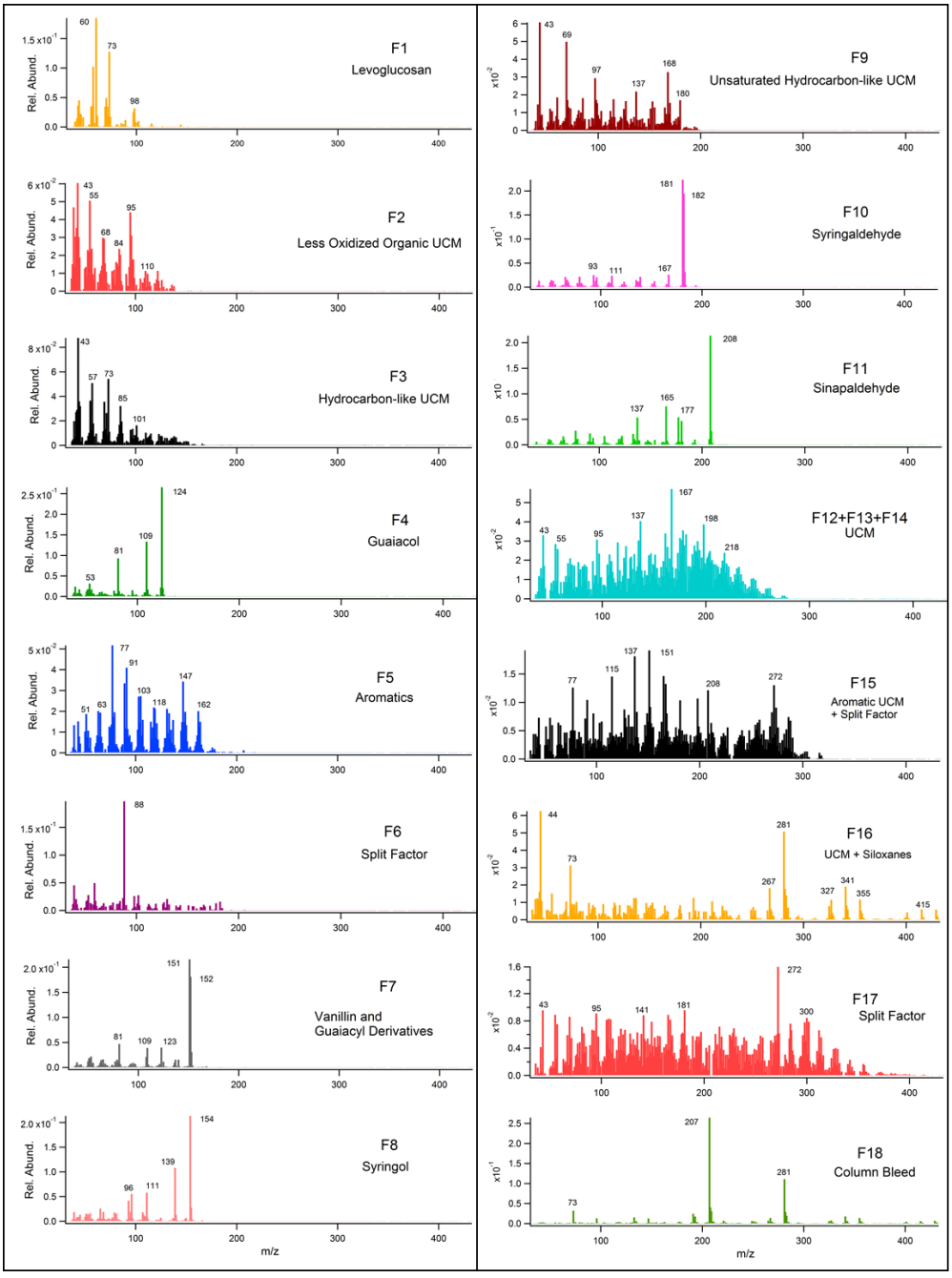

Figure 7: Mass spectra for factors 1-18 (F1-18) in PMF 18-factor solution on TAG oak wood BBOA compound window data. Relevant plots obtained in PMF calculations are provided in Supplemental Information (Figures 9b and 10b).

Atmos. Chem. Phys. Discuss., https://doi.org/10.5194/acp-2017-576
Manuscript under review for journal Atmos. Chem. Phys.
Discussion started: 5 July 2017

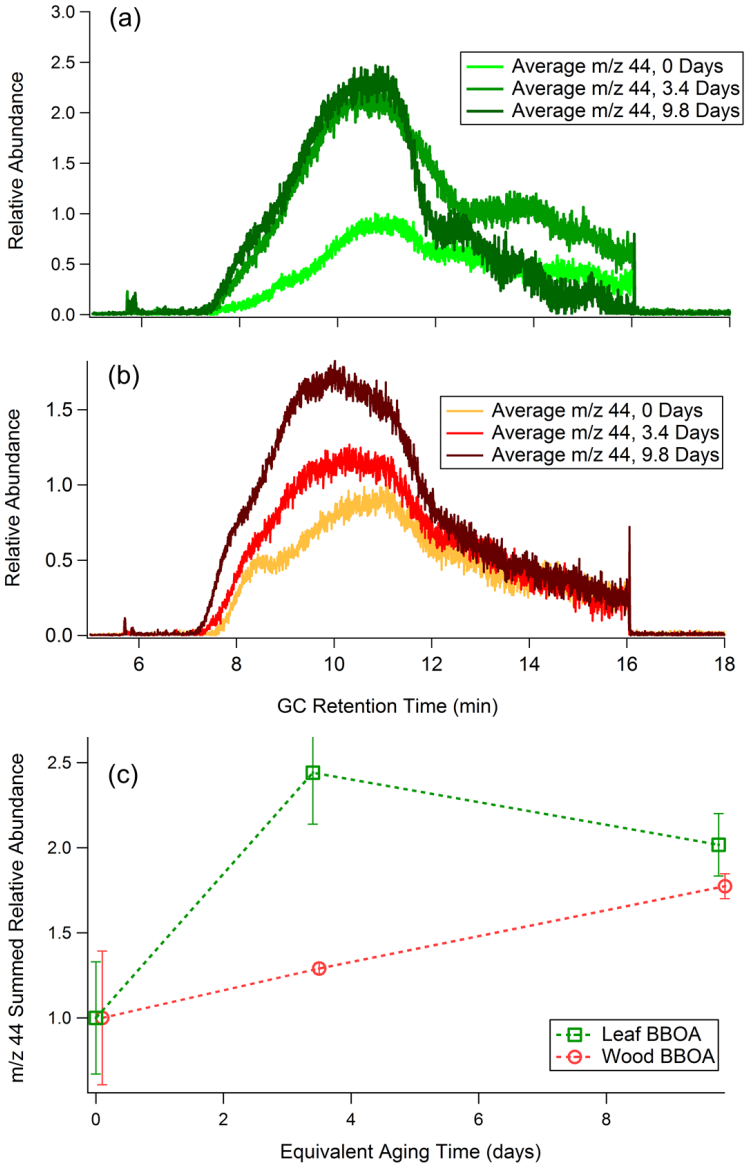

Figure 8: (a) Average *m/z* 44 single ion chromatograms (SICs) across different levels of photochemical aging for leaf BBOA, normalized to the point of highest abundance within the averaged unaged chromatogram ("0 days"). **(b)** Average *m/z* 44 single ion chromatograms (SICs) across different levels of photochemical aging for wood BBOA, normalized to the point of highest abundance within the averaged unaged chromatogram. **(c)** summed relative *m/z* 44 decomposition signal as a function of photochemical aging for both fuels (± one standard deviation). These values were obtained by averaging triplicate *m/z* 44 decomposition signals at each level of photochemical aging. For each fuel type, all summed abundances are normalized to the unaged *m/z* 44 signal ("0 days").

Atmos. Chem. Phys. Discuss., https://doi.org/10.5194/acp-2017-576
Manuscript under review for journal Atmos. Chem. Phys.
Discussion started: 5 July 2017

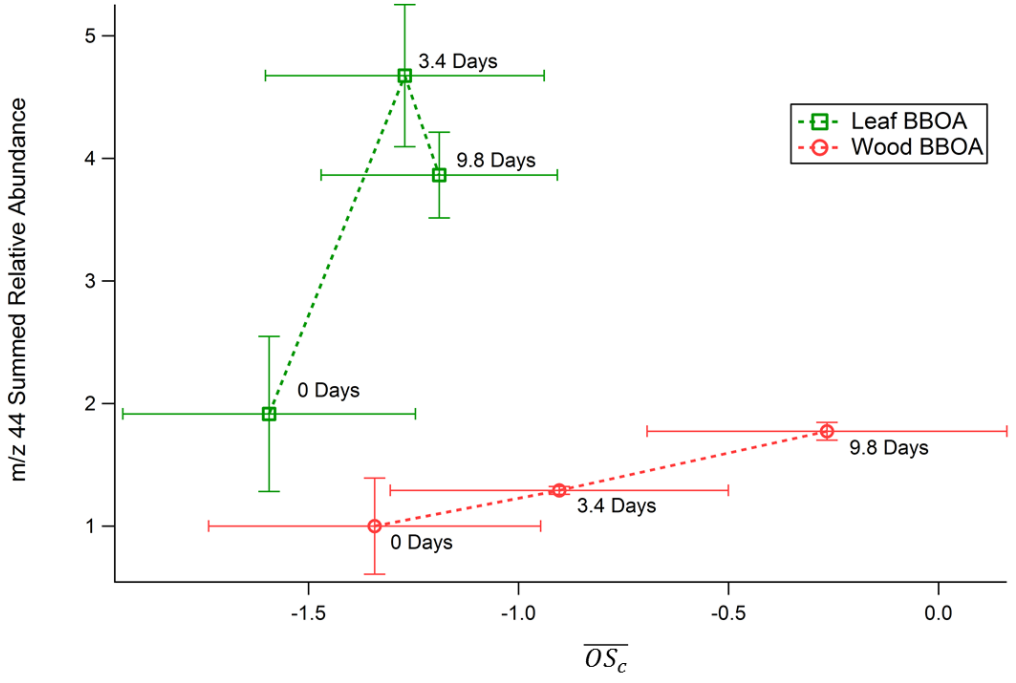

Figure 9: TAG decomposition *m/z* 44 integrated relative abundances for PAM-aged wood and leaf BBOA as functions of AMS $\overline{OS_c}$. Here, all TAG data have been normalized to the unaged (0 days) wood BBOA integrated *m/z* 44 abundance.

Atmos. Chem. Phys. Discuss., https://doi.org/10.5194/acp-2017-576
Manuscript under review for journal Atmos. Chem. Phys.
Discussion started: 5 July 2017

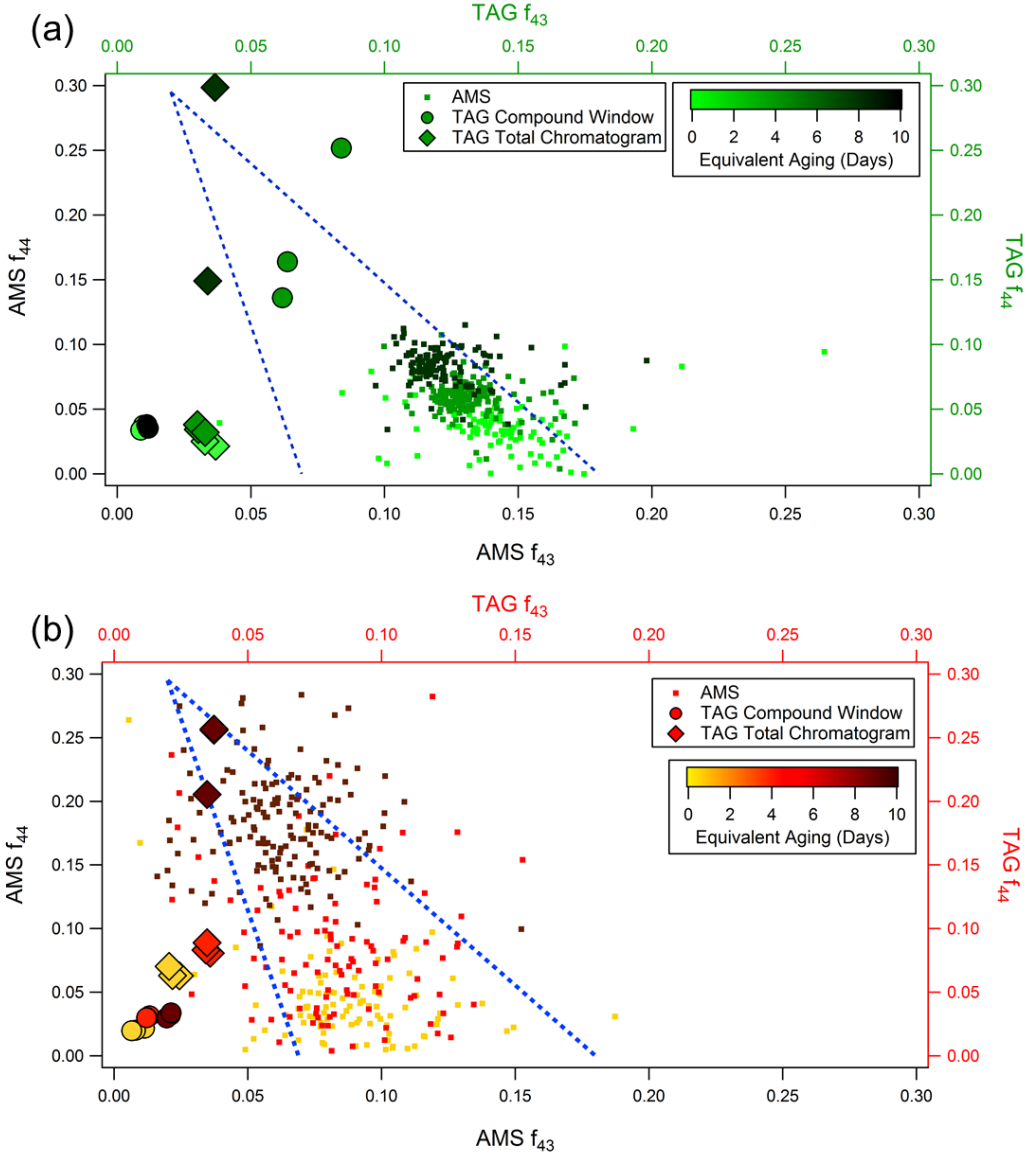

Figure 10: AMS and TAG f_{44} vs f_{43} at different levels of photochemical aging for **(a)** oak leaf and **(b)** oak wood BBOA. TAG f_{44} and f_{43} values were obtained using Eq. (1). To minimize noise, AMS data is plotted only for points where sufficient total organic concentrations were achieved, around the peak of the concentration profile. The blue dotted lines provide guidelines for the eye where data points tend to be concentrated.

Atmos. Chem. Phys. Discuss., https://doi.org/10.5194/acp-2017-576
Manuscript under review for journal Atmos. Chem. Phys.
Discussion started: 5 July 2017

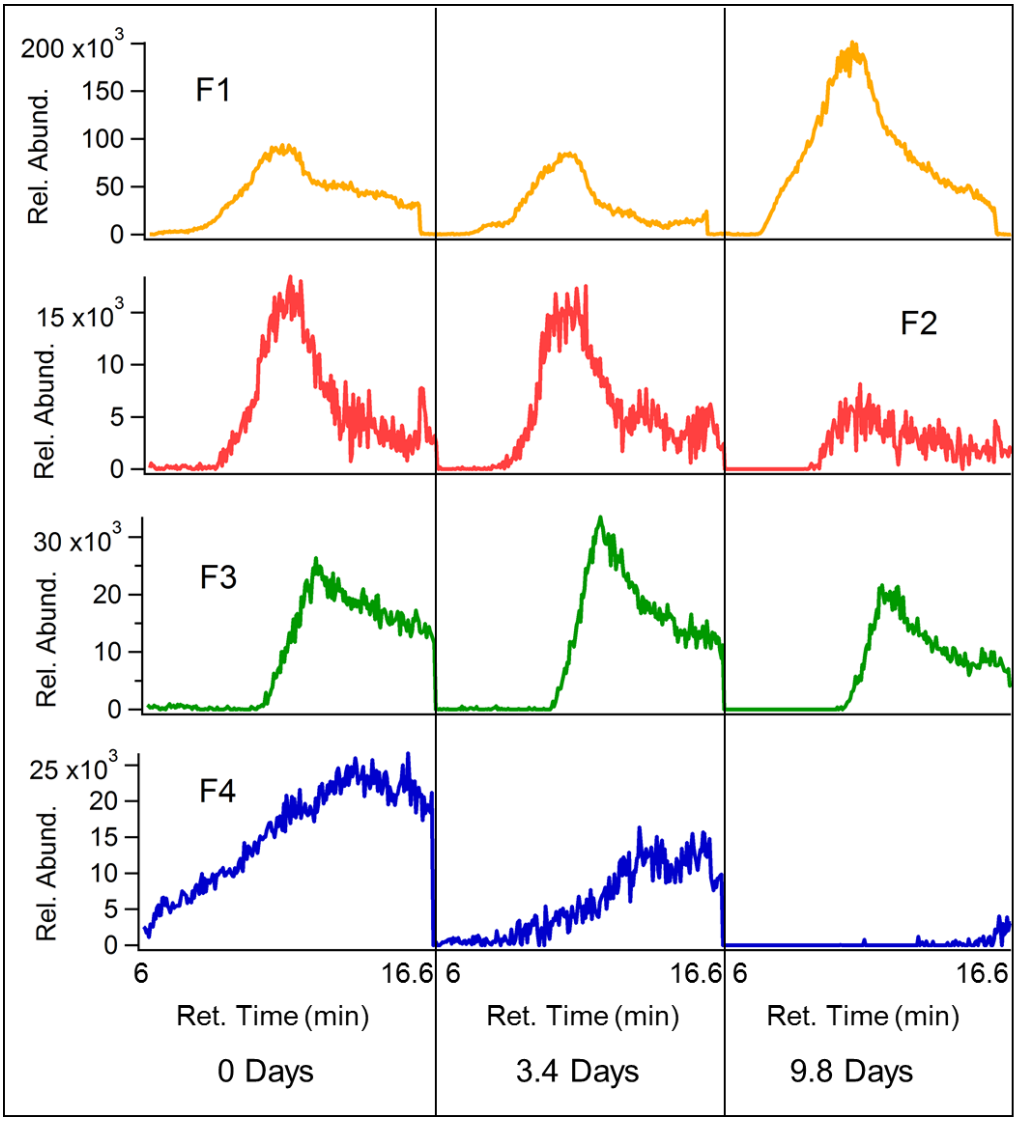

Figure 11: Average binned chromatograms for factors 1-4 (F1-4) in PMF 4-factor solution on TAG oak leaf BBOA decomposition window data. Relevant plots obtained in PMF calculations are provided in Supplemental Information (Figures 9c and 10c). These chromatograms were obtained from PMF calculations by averaging binned data corresponding to triplicate chromatograms at each level of oxidation. The triplicate-averaged binned chromatograms at each equivalent aging time are displayed in one trace; different aging times are demarcated with vertical lines across the x-axis.

Atmos. Chem. Phys. Discuss., https://doi.org/10.5194/acp-2017-576
Manuscript under review for journal Atmos. Chem. Phys.
Discussion started: 5 July 2017

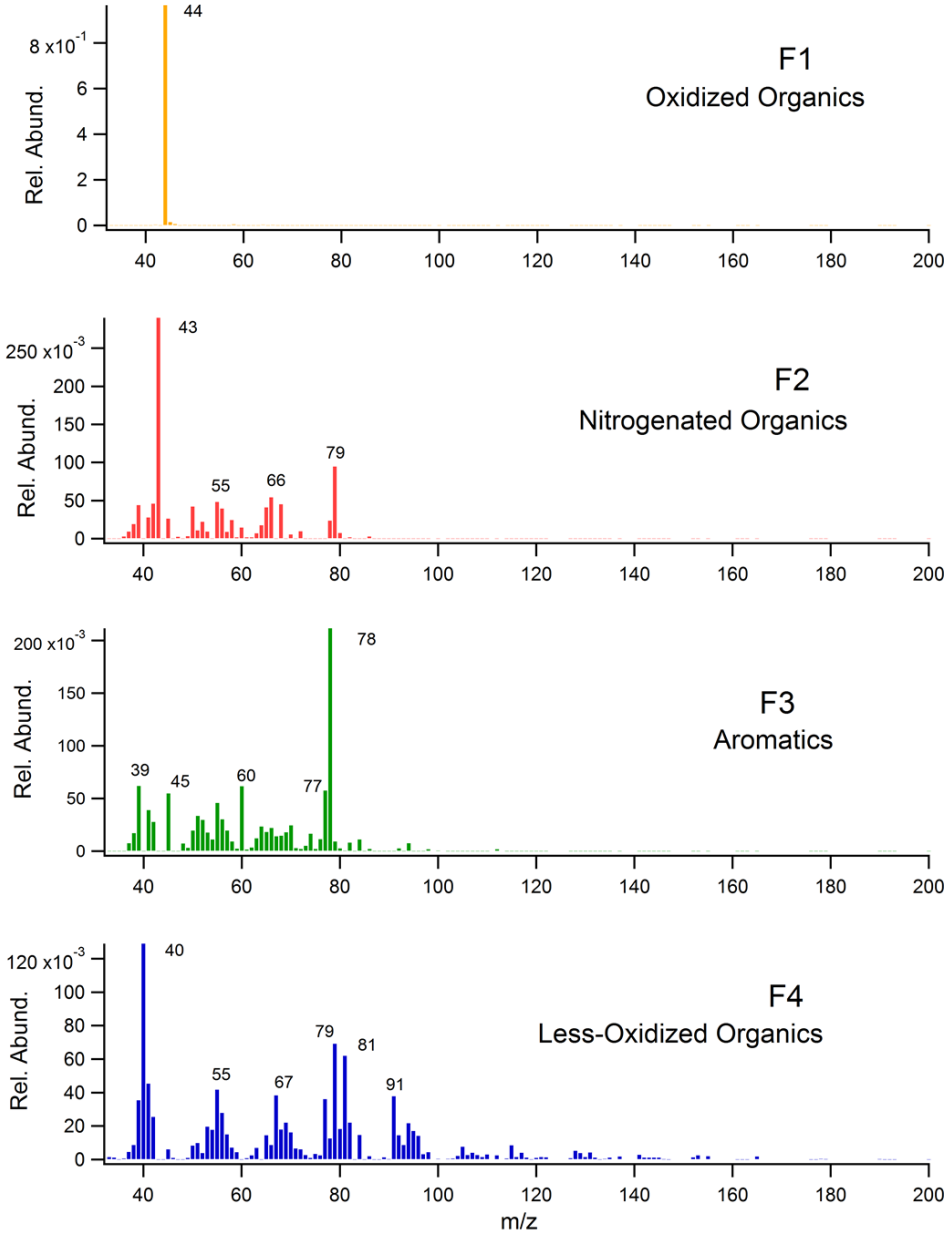

910 **Figure 12:** Mass spectra for factors 1-4 (F1-4) in PMF 4-factor solution on TAG oak leaf BBOA decomposition window data. Relevant plots obtained in PMF calculations are provided in Supplemental Information (Figures 9c and 10c).

Atmos. Chem. Phys. Discuss., https://doi.org/10.5194/acp-2017-576
Manuscript under review for journal Atmos. Chem. Phys.
Discussion started: 5 July 2017

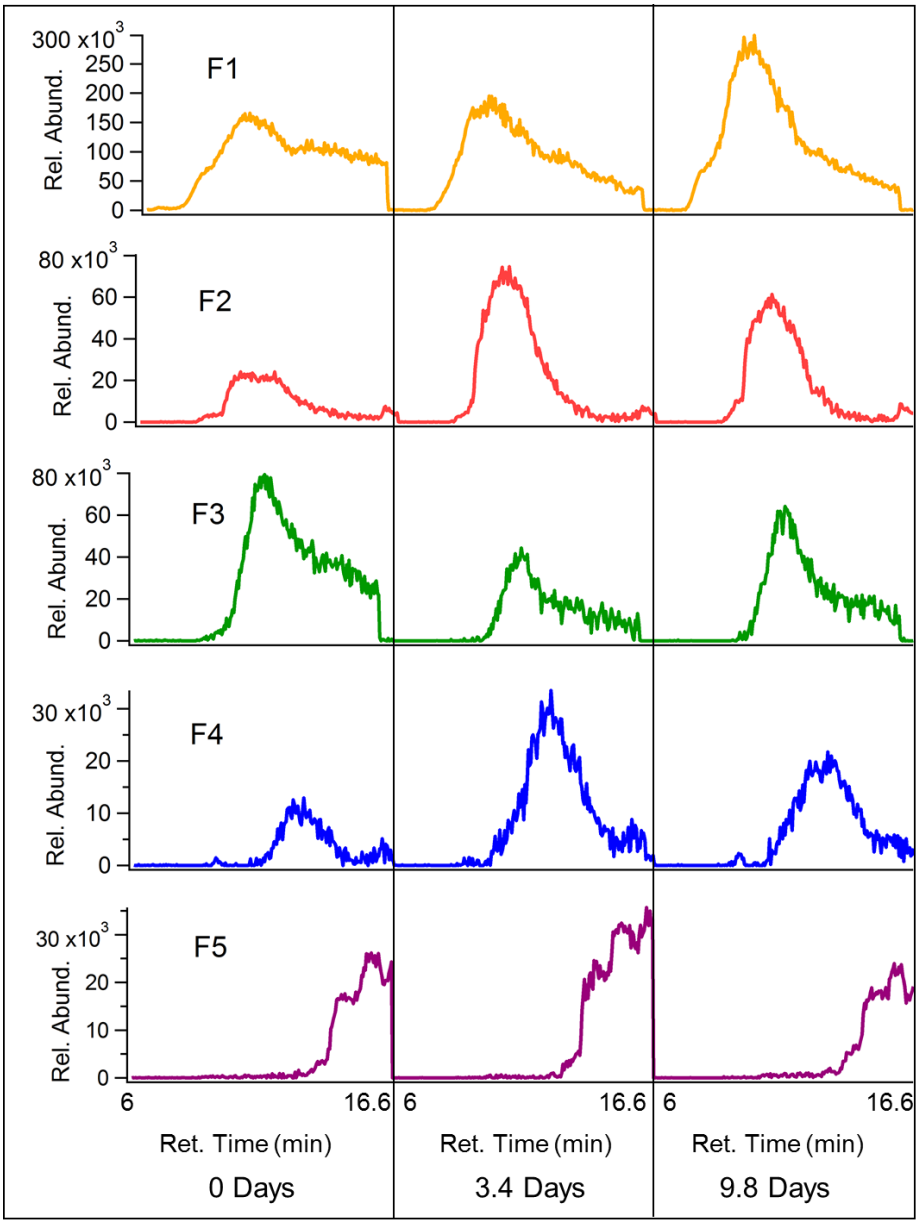

915 **Figure 13.** Average binned chromatograms for factors 1-5 (F1-5) in PMF 5-factor solution on TAG oak wood BBOA decomposition window data. Relevant plots obtained in PMF calculations are provided in Supplemental Information (Figures 9d and 10d). These chromatograms were obtained from PMF calculations by averaging binned data corresponding to triplicate chromatograms at each level of oxidation. The triplicate-averaged binned chromatograms at each equivalent aging time are displayed in one trace; different aging times are demarcated with vertical lines along
920 the x-axis.

Atmos. Chem. Phys. Discuss., https://doi.org/10.5194/acp-2017-576
Manuscript under review for journal Atmos. Chem. Phys.
Discussion started: 5 July 2017

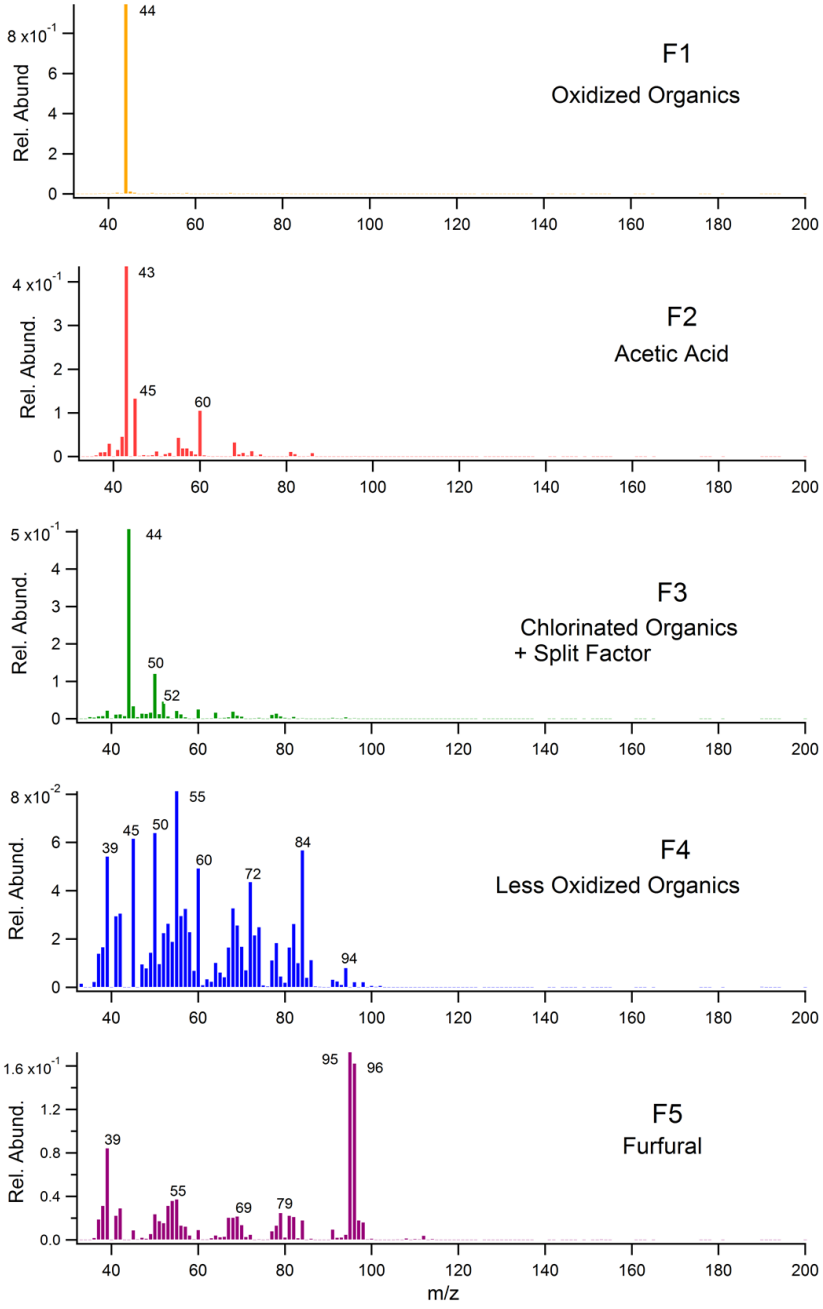

Figure 14: Mass spectra for factors 1-5 (F1-5) in PMF 5-factor solution on TAG oak leaf BBOA decomposition window data. Relevant plots obtained in PMF calculations are provided in Supplemental Information (Figures 9d and 10d).

Atmos. Chem. Phys. Discuss., https://doi.org/10.5194/acp-2017-576
Manuscript under review for journal Atmos. Chem. Phys.
Discussion started: 5 July 2017

Atmospheric Chemistry and Physics Discussions

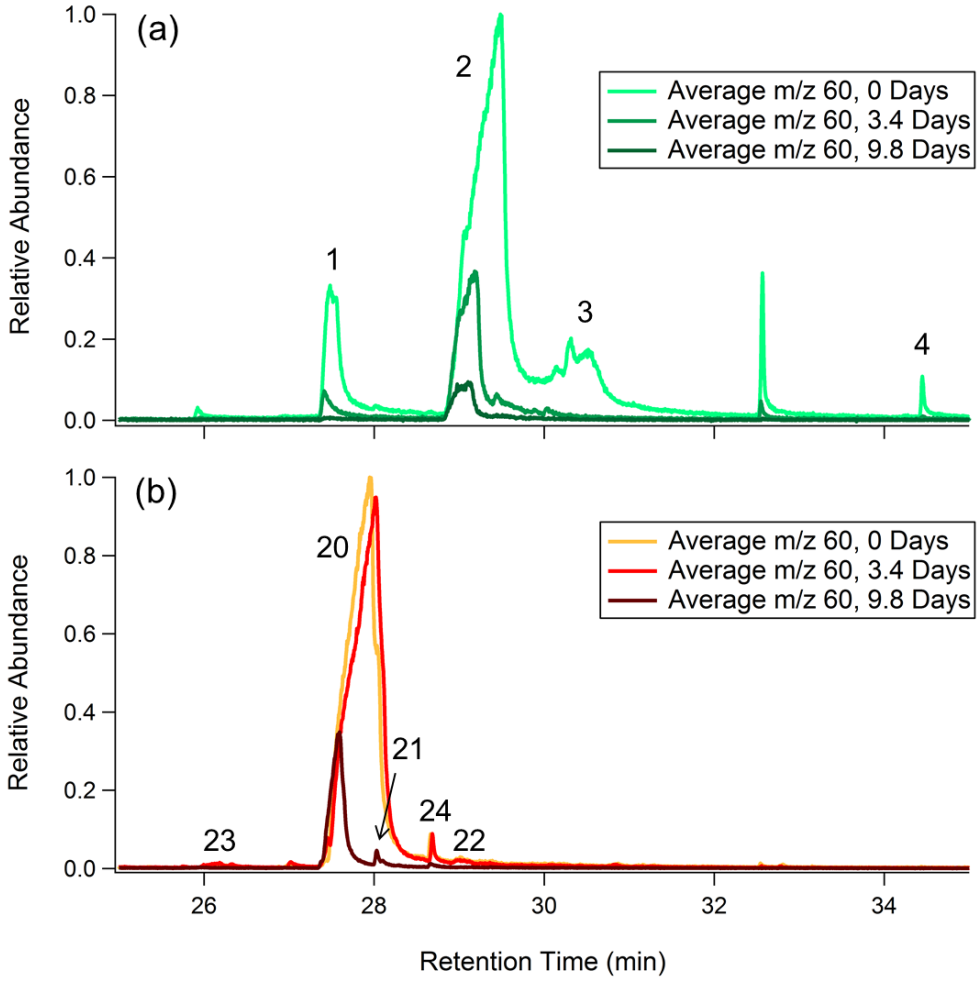

925

Figure 15: Average *m/z* 60 single ion chromatograms (SICs) across the compound window for **(a)** leaf BBOA; **(b)** wood BBOA. For each plot, all traces are normalized to the point of highest abundance within the average unaged chromatogram. Individual compounds are labeled according to identifications provided in Supplemental Information (Figures S5 and S6; Tables S3 and S4).

930

Atmos. Chem. Phys. Discuss., https://doi.org/10.5194/acp-2017-576
Manuscript under review for journal Atmos. Chem. Phys.
Discussion started: 5 July 2017

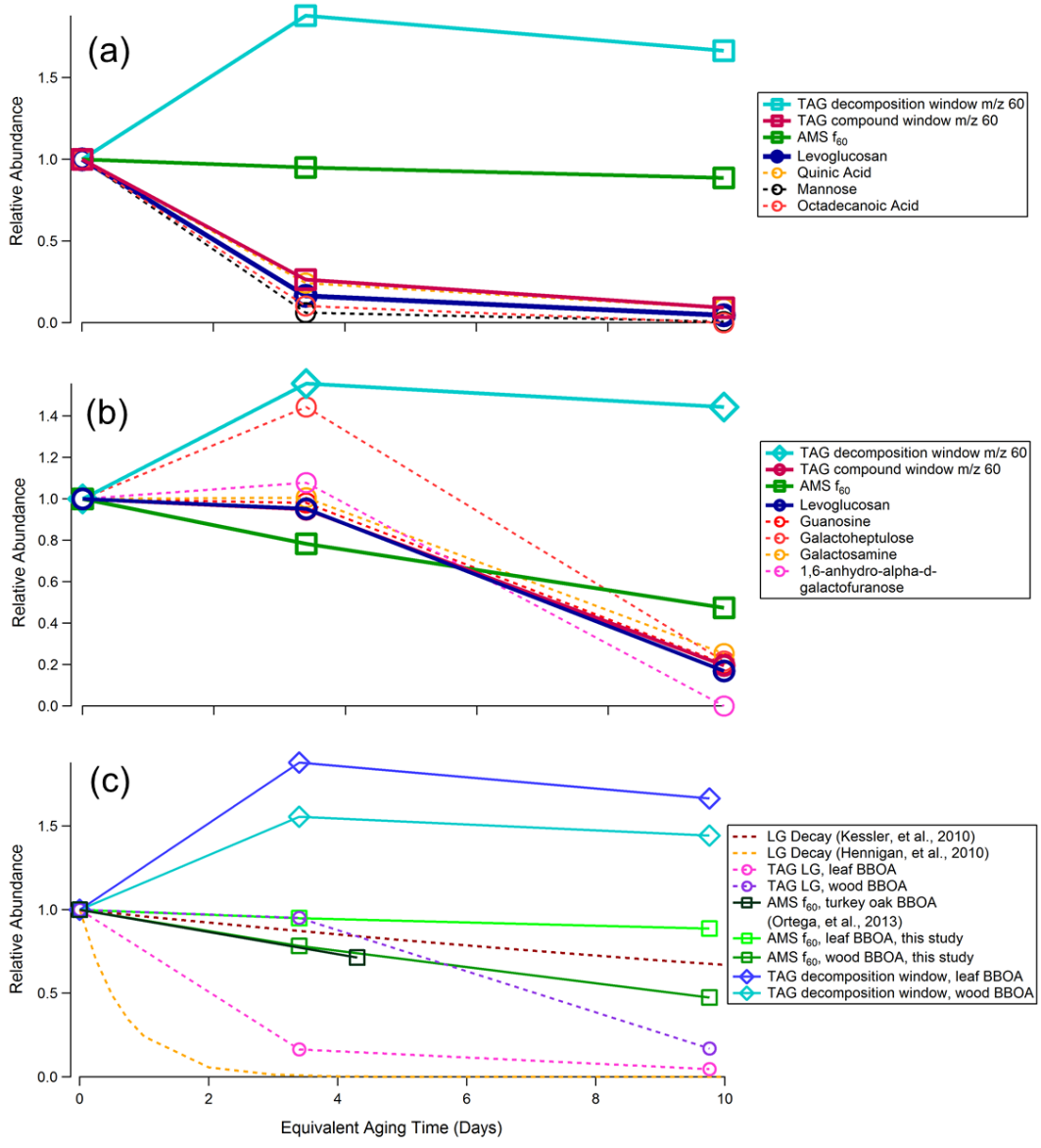

Figure 16. Relative changes in abundance for different *m/z* 60 fragmenting species in **(a)** leaf and **(b)** wood BBOA; **(c)** TAG and AMS *m/z* 60 species as a function of OH_{exp}. Levoglucosan (LG) decay rates were calculated using two different literature k_{LG} values (Hennigan et al., 2010; Kessler et al., 2010) with an assumed typical outdoor OH· concentration of 1.5×10^{-6} molec cm^{-3} (Mao et al., 2009). Additionally, normalized AMS f_{60} values for turkey oak (*Quercus laevis*) BBOA obtained during the FLAME-3 campaign were adapted from Figure 10b in Ortega, et al. (Ortega et al., 2013) and are included for comparison.

Atmos. Chem. Phys. Discuss., https://doi.org/10.5194/acp-2017-576
Manuscript under review for journal Atmos. Chem. Phys.
Discussion started: 5 July 2017

Atmospheric Chemistry and Physics Discussions

Table 1. Qualitative levels of PAM-reactor oxidation with corresponding OH· exposure (OH_{exp}) estimations and equivalent aging times.

Qualitative Level of Oxidation	OH_{exp} (molec cm^{-3} s)	Equivalent Aging Time (days)
low-mid	4.41×10^{11}	3.4
high	1.26×10^{12}	9.8

940